Manuscript prepared for Atmos. Chem. Phys.
with version 2015/09/17 7.94 Copernicus papers of the LaTeX class copernicus.cls.
Date: 2 June 2016

Growth of nucleation mode particles in the summertime Arctic: a case study

Megan D. Willis[1], Julia Burkart[1], Jennie L. Thomas[2], Franziska Köllner[3], Johannes Schneider[3], Heiko Bozem[4], Peter M. Hoor[4], Amir A. Aliabadi[5,a], Hannes Schulz[6], Andreas B. Herber[6], W. Richard Leaitch[5], and Jonathan P.D. Abbatt[1]

[1]University of Toronto, Department of Chemistry, Toronto, Ontario, Canada
[2]LATMOS/IPSL, UPMC Univ. Paris 06 Sorbonne Universités, UVSQ, CNRS, Paris, France
[3]Max Planck Institute for Chemistry, Particle Chemistry Department, Mainz, Germany
[4]Johannes Gutenberg University of Mainz, Institute for Atmospheric Physics, Mainz, Germany
[5]Environment and Climate Change Canada, Toronto, Ontario, Canada
[6]Alfred Wegener Institute Helmholtz-Center for Polar and Marine Research Bremerhaven, Bremerhaven, Germany
[a]Now at: Massachusetts Institute of Technology, Department of Architecture, Cambridge, USA

Correspondence to: Megan D. Willis (megan.willis@mail.utoronto.ca)

Abstract. The summertime Arctic lower troposphere is a relatively pristine, background aerosol environment dominated by nucleation and Aitken mode particles. Understanding the mechanisms that control the formation and growth of aerosol is crucial for our ability to predict cloud properties, and therefore radiative balance and climate. We present an analysis of an aerosol growth event observed in the Canadian Arctic Archipelago during summer as part of the NETCARE project. Under stable and clean atmospheric conditions, with low inversion heights, carbon monoxide less than 80 $\mathrm{ppb_v}$ and black carbon less than 5 $\mathrm{ng\,m^{-3}}$, we observe growth of small particles, <20 nm in diameter, into sizes above 50 nm. Aerosol growth was correlated with the presence of organic species, trimethylamine and methanesulfonic acid (MSA) in particles ∼80 nm and larger, where the organics are similar to those previously observed in marine settings. MSA-to-sulfate ratios as high as 0.15 were observed during aerosol growth, suggesting an important marine influence. The organic-rich aerosol contributes significantly to particles active as cloud condensation nuclei (CCN, supersaturation = 0.6%), which are elevated in concentration during aerosol growth above background levels of ∼100 $\mathrm{cm^{-3}}$ to ∼220 $\mathrm{cm^{-3}}$. Results from this case study highlight the potential importance of secondary organic aerosol formation and its role in growing nucleation mode aerosol into CCN-active sizes in this remote marine environment.

1 Introduction

In the warming Arctic (Jeffries and Richter-Menge, 2012), decreasing sea ice extent (Lindsay et al., 2009) is likely to increase the oceanic influence on atmospheric composition. This change in exposed ocean area will have implications on aerosol concentrations and composition, and therefore on cloud properties (Browse et al., 2014) and precipitation (Kopec et al., 2016). Aerosol-cloud-climate interactions are unique in Arctic regions due to the high surface albedo, the seasonal cycle in aerosol loading and properties, the strong static stability in the lower troposphere (Aliabadi et al., 2016b) and the dependence of cloud infrared emissivity on droplet size and aerosol characteristics (Curry, 1995).

Pristine, background aerosol conditions prevail in the summertime Arctic boundary layer. A pronounced seasonal cycle characterizes Arctic aerosol (Engvall et al., 2008; Sharma et al., 2013; Tunved et al., 2013; Croft et al., 2015; Nguyen et al., 2016), with strong anthropogenic contributions to "Arctic Haze" in winter and spring (Law and Stohl, 2007; Quinn et al., 2007), and more regional influences in the cleaner summer months, especially in the lower troposphere (Leaitch et al., 2013; Heintzenberg et al., 2015). Beginning in late spring, efficient wet removal of aerosol and less efficient transport from lower latitudes come together to suppress the condensation sink (Stohl, 2006; Engvall et al., 2008) and allow nucleation and Aitken mode particles to dominate the size distribution (Engvall et al., 2008; Heintzenberg and Leck, 2012; Croft et al., 2015). Under these clean conditions cloud condensation nuclei (CCN) and cloud droplet number concentrations can be exceptionally low (Mauritsen et al., 2011; Leaitch et al., 2016), making summertime liquid clouds very sensitive to the formation of new particles and their growth into CCN sizes. Since Arctic clouds are an important determinant of the local surface energy balance (e.g., Intrieri et al., 2002; Lubin and Vogelmann, 2006) and have the ability to influence the thickness, freezing and melting of sea ice (Kay and Gettelman, 2009; Tjernström et al., 2015), a predictive understanding of the sources and processes controlling CCN-active aerosol is a crucial aspect of understanding the Arctic climate.

While transport of pollutants from lower latitudes does occur in Arctic summer, especially in the middle and upper troposphere, efficient scavenging during transport and within Arctic regions results in an important contribution from regional sources near the surface at this time of year (e.g., Stohl, 2006; Garrett et al., 2011; Croft et al., 2015). In the absence of significant transported aerosol, several different processes can contribute to aerosol formation, including the emission of primary particles from the ocean surface, along with formation of new particles by nucleation and their subsequent growth by condensation and coagulation.

The formation of new particles can be an important aerosol source in the summertime Arctic (Leaitch et al., 2013; Croft et al., 2015). Through its oxidation to sulfuric acid and other products, dimethyl sulfide (DMS) plays an important role in the formation, and growth, of new particles (Leaitch et al., 2013). In the Arctic and at mid-latitudes, uncertainties in the rates and mechanisms of nucleation and growth are such that some studies are able to explain ambient observations with standard parametrizations developed from measurements at more southerly locations (e.g., Chang et al., 2011b), while others must invoke alternative mechanisms (e.g., Karl et al., 2012). The role of ammonia and amines in particle nucleation at mid-latitudes has become well established (Almeida et al., 2013), and recent measurements suggest that local ammonia sources in the summer Arctic are sufficient to promote particle formation (Wentworth et al., 2015; Giamarelou et al., 2016). Iodine oxides can make a significant contribution to new particle formation in marine and coastal environments at mid-latitudes (e.g., O'Dowd and de Leeuw, 2007); these species may contribute to the formation and growth of small particles in Arctic regions, although their biotic and abiotic sources in ice-covered regions remain unclear (Mahajan et al., 2010; Allan et al., 2015). Organic condensible species also play a role in nucleation, and growth, of particles at mid-latitudes (e.g., Kulmala and Kerminen, 2008; Metzger et al., 2010; Ehn et al., 2014); however, no direct evidence for the role of organic species in Arctic nucleation events exists to date.

The ejection of primary aerosol from the sea surface, through wave-breaking and bubble-bursting, is another source of aerosol across the size distribution (Ovadnevaite et al., 2014; Clarke et al., 2006; Nilsson et al., 2001). At mid-latitudes a large organic fraction, which originates from the enrichment of biologically-derived organic material at the sea surface, is frequently observed in marine aerosol (Facchini et al., 2008b; Gantt and Meskhidze, 2013; Frossard et al., 2014; Quinn et al., 2015a; O'Dowd et al., 2015; Quinn et al., 2015b). This primary marine organic aerosol (OA) tends to be water-insoluble with chemical similarity to lipids (e.g., Rinaldi et al., 2010; Decesari et al., 2011), and has been demonstrated to have a source near the ocean surface (Ceburnis et al., 2008). Some similar observations have been made in Arctic regions (e.g., Narukawa et al., 2008; Orellana et al., 2011; Fu et al., 2013; Karl et al., 2013; Fu et al., 2015). For example, Fu et al. (2013, 2015) have shown a dominance of primary saccharides and evidence for protein and humic-like substances in Arctic aerosol suggesting an important local or regional source of primary marine OA. The release of marine micro-gels via bubble-bursting in open leads has been proposed to contribute significantly to particles over the Arctic Ocean (e.g., Bigg and Leck, 2001; Orellana et al., 2011).

Particle growth through condensation of gas-phase species can also play a role in driving marine aerosol characteristics, making ambient marine OA a complex result of primary and secondary processes (e.g., Ceburnis et al., 2008; Facchini et al., 2008b; Rinaldi et al., 2010; Frossard et al., 2014). In contrast to primary marine OA, secondary marine OA is generally more water-soluble and is composed of more oxygenated compounds (Rinaldi et al., 2010; Decesari et al., 2011). Precursors of secondary marine OA include DMS and other biological volatile organic compounds (BVOCs), such as isoprene, monoterpenes and amines, which are produced by a variety of marine micro-organisms (Shaw et al., 2010; Gantt et al., 2009; Facchini et al., 2008a). However, in the absence of specific molecular tracers it can be very challenging to discern the relative contribution of primary and secondary processes to ambient marine organic aerosol (e.g., O'Dowd et al., 2015). At mid-latitudes, direct and indirect measurements of Aitken mode particle composition have demonstrated the role of secondary organic species in the growth of small particles (Vaattovaara et al., 2006; Bzdek et al., 2014; Lawler et al., 2014). Significant fractions of alkylamines, dicarboxylic acids, methansulfonic acid, oxalic acid, alcohols and other organic acids have been observed in marine aerosol, suggesting contributions from secondary processes (e.g., Facchini et al., 2008a; Claeys et al., 2010; Rinaldi et al., 2010; Dall'Osto et al., 2012; Frossard et al., 2014). In Arctic regions, the detection of specific molecular tracers for isoprene, terpene and fatty acid oxidation have indicated a contribution of secondary processes to summertime organic aerosol (Fu et al., 2009; Kawamura et al., 2012; Fu et al., 2013; Hansen et al., 2014).

Our understanding of summertime Arctic aerosol remains incomplete, in part due to a scarcity of observations focusing on the influence of local and regional sources on aerosol chemical and physical properties. In this case study we focus on observations of a new particle formation and growth event made during the NETCARE summer aircraft campaign in July 2014, near Resolute Bay, Nunavut, Canada, in a general time period and location that was shown to have high biological activity in the surface ocean (Gosselin et al., 2015; Mungall et al., 2015). We use these observations to explore the composition and formation processes of particles contributing to cloud condensation nuclei in the Canadian Arctic Archipelago during summer.

2 Methods

2.1 Measurement platform and inlets

As part of the NETCARE project (Network on Climate and Aerosols: Addressing Key Uncertainties in Remote Canadian Environments, http://www.netcare-project.ca), measurements of aerosol physical and chemical properties, trace gases and meteorological parameters were made aboard the Alfred Wegener Institute (AWI) Polar 6 aircraft; a DC-3 aircraft converted to a Basler BT-67 (Herber et al., 2008). Measurements aboard Polar 6 took place from July 4 – 21, 2014, based in Resolute Bay, Nunavut (74° 41' N, 94° 52' W). The survey speed was maintained at approximately ~~120 (~~$\sim$ ~~222)~~ 75 $\mathrm{m\,s^{-1}}$ for measurement flights, with ascent and descent rates of 150 $\mathrm{m\,min^{-1}}$ for vertical profiles.

The main aerosol inlet was located on the starboard side of the fuselage ahead of the engines. Based upon a total flow drawn to instruments of 35 $\mathrm{L\,min^{-1}}$ and a measured flow at the exhaust of the sampling line of 20 $\mathrm{L\,min^{-1}}$, the total flow through the shrouded inlet diffuser was nearly isokinetic at 55 $\mathrm{L\,min^{-1}}$. Aerosol flowed into the cabin through a stainless steel manifold (outer diameter = ~~1.9~~2.5 cm, inner diameter = 2.3 cm) and was directed to the various particle instruments through stainless steel lines that branched from the main inlet at angles less than 90 degrees. Aerosol was not dried prior to sampling; however, the temperature in the inlet line was approximately 10 – 15 °C warmer than the ambient temperature so that the relative humidity (RH) decreased significantly as the aerosol entered the sampling line. Exhaust from the main aerosol inlet flowed freely into the back of the cabin to keep the inlet from being over-pressured. Therefore, the total flow through the main aerosol inlet was dictated by the true airspeed (TAS). With the survey air speed noted above, transmission efficiency of aerosol through the main inlet was near unity for particles 20 nm to $\sim$1 µm in diameter.

Trace gases (CO, CO_2 and H_2O) were sampled through a second inlet consisting of a 0.40 cm (outer diameter) Teflon line, with a continuously measured sample of flow of $\sim$ 12 $\mathrm{L\,min^{-1}}$. The trace gas inlet used the forward motion of the aircraft to push ambient air into the line in combination with a rear-facing 0.95 cm Teflon exhaust line that lowered the pressure in the sampling line.

2.2 State parameters and winds

State parameters and meteorological conditions were measured with an AIMMS-20, manufactured by Aventech Research Inc. (Barrie, Ontario, Canada http://aventech.com/products/aimms20.html). The AIMMS-20 consists of three modules: (1) an Air Data Probe, which measures temperature and the three-dimensional aircraft-relative flow vector (TAS, angle-of-attack and side-slip) with a three-dimensional accelerometer for measurement of turbulence; (2) an Inertial Measurement Unit, which provides the aircraft angular rate and acceleration; (3) a Global Positioning System for aircraft three-dimensional position and inertial velocity. Vertical and horizontal wind speeds are measured with accuracies of 0.75 and 0.50 $\mathrm{m\,s^{-1}}$, respectively. Accuracy and precision of the temperature measurement are 0.30 and 0.10 $^{\circ}\mathrm{C}$, respectively.

2.3 Aerosol physical properties

Measurements of particle number concentrations, and size, were made aboard Polar 6 at a frequency of 1 Hz, unless otherwise indicated. Number concentrations of particles greater than 5 nm in diameter ($N_{>5}$) were measured with a TSI 3787 water-based ultra-fine condensation particle counter (UCPC), sampling at a flow rate of 0.6 $\mathrm{L\,min^{-1}}$. Aerosol number size distributions from 20 nm to 1 $\mathrm{\mu m}$ were acquired with two instruments: a Brechtel Manufacturing Incorporated (BMI) Scanning Mobility System (SMS) coupled to a TSI 3010 Condensation Particle Counter (CPC) measured from 20 to 100 nm (N_{20-100}) with a 60-second time resolution, while a Droplet Measurement Technology (DMT) Ultra High Sensitivity Aerosol Spectrometer (UHSAS) measured number size distributions from 70 nm to 1 $\mathrm{\mu m}$ ($N_{>70}$) with a time resolution of 1 Hz. The SMS sampled at a flow rate of 1 $\mathrm{L\,min^{-1}}$, with a dried (∼20% RH) sheath flow of 6 $\mathrm{L\,min^{-1}}$. The UHSAS uses light scattering signals from a 1054 nm laser for particle detection and sizing on a single-particle basis (e.g., Cai et al., 2008), with a sample flow rate of 55 $\mathrm{cm^3\,min^{-1}}$ from a bypass flow off the main aerosol inlet. Characterization and calibration of the UCPC, SMS, ~~UHSAS and CCNC~~ and UHSAS are described in detail in Leaitch et al. (2016). ~~Agreement between the particle instruments was generally~~ Particle number concentrations from the SMS and UHSAS generally agreed within a factor of two over their overlapping size range (70 to 100 nm).

Particle number concentrations from all instruments are reported at ambient pressure and temperature. A characteristic size distribution is shown in Figure 1. Values of $N_{>80}$, $N_{>100}$ and $N_{>200}$ were derived from UHSAS measurements. Number concentrations from 5 to 20 nm (N_{5-20}) were estimated by subtracting the sum of the SMS total number concentration (N_{20-100}) and UHSAS $N_{>100}$

from the total UCPC concentration (i.e., $N_{>5}$). The number of particles greater than 50 nm ($N_{>50}$) was determined by the sum of the SMS number from 50 to 100 nm (N_{50-100}) and the UHSAS $N_{>100}$. Here, we refer to N_{5-20} as the nucleation mode, N_{20-100} as the Aitken mode and $N_{>100}$ and larger as the accumulation mode.

2.4 Cloud condensation nuclei concentrations

Cloud Condensation Nuclei (CCN) concentrations were measured using a DMT CCN counter (CCNC, Model 100), sampling behind a DMT pressure controlled inlet at a reduced pressure of ~650 hPa. The effective supersaturation (for a nominal water supersaturation of 1%, at 650 hPa) was found to be 0.6% (Leaitch et al., 2016), and was held constant throughout the study to allow more measurement stability and the highest time resolution possible, and to examine the hygroscopicity of small particles. Calibration and characterization of the CCNC is described in (Leaitch et al., 2016).

The effective aerosol hygroscopicity parameter (κ) was estimated according to Petters and Kreidenweis (2007), using the average aerosol composition from the aerosol mass spectrometer (see below) with ammonium sulfate and organic aerosol densities of 1770 $\mathrm{kg\,m^{-3}}$ and 1550 $\mathrm{kg\,m^{-3}}$, respectively (e.g., Chang et al., 2010). Assuming a temperature of 298 K and the surface tension of pure water the dry diameter for activation was calculated at the supersaturation of our CCN measurements. The measured size distribution could then be integrated down to this dry diameter to produce predicted CCN concentrations for comparison with measured values.

2.5 Trace gases

Carbon monoxide (CO) concentrations were measured with an Aerolaser ultra-fast carbon monoxide monitor (model AL 5002), based on VUV-fluorimetry using excitation of CO at 150 nm. The instrument was modified such that in-situ calibrations could be conducted in flight. CO concentrations are used here as a relative indicator of aerosol influenced by pollution sources, such as anthropogenic or biomass burning emissions.

Water vapour (H_2O) measurements were based on infrared absorption using a LI-7200 enclosed CO_2/H_2O Analyzer from LI-COR Biosciences GmbH. In-situ calibrations were performed during flight at regular intervals (15 – 30 min) using a NIST traceable CO_2 standard with zero water vapor concentration. The measurement uncertainty is $\pm$ 40 $\mathrm{ppm_v}$. H_2O mixing ratios were used to calculate relative humidity with pressure and temperature measured by the AIMMS-20.

2.6 Sub-micron aerosol composition

2.6.1 Single particle soot photometer

Concentrations of refractory black carbon (rBC) containing particles were measured with a DMT single particle soot photometer (SP2) (described in Schwarz et al. (2006) and Gao et al. (2007)), and are used as an indicator of pollution influences. The SP2 uses a continuous intra-cavity Nd:YAG laser (1064 nm) to classify particles as either incandescent (rBC) or scattering (non-rBC), based on the individual particle's interaction with the laser beam. The peak incandescence signal is linearly related to the rBC mass. The SP2 was calibrated with an Aquadag standard by selecting a narrow size distribution of particles with a differential mobility analyzer upstream of the SP2 (Schwarz et al., 2006; Laborde et al., 2012). The detection efficiency of this SP2 (version D) drops off for particles smaller than 70 nm. A log-normal fit through the mass-size distribution indicates that the SP2 measured 92% of the total ambient rBC mass. Reported rBC values were thus scaled up by a factor of 1.08 to account for the fraction of rBC particles that were outside of the SP2 detection range. The SP2 sampled at 120 $\mathrm{cm}^3\,\mathrm{min}^{-1}$, sharing a bypass line from the main aerosol inlet with the UHSAS.

2.6.2 Aerosol mass spectrometer

Sub-micron aerosol composition was measured with an Aerodyne high-resolution time-of-flight aerosol mass spectrometer (HR-ToF-AMS), described in detail by DeCarlo et al. (2006). The HR-ToF-AMS deployed here was equipped with an infrared laser vaporization module similar to that of the SP2 (DMT); however, measurements of refractory black carbon (rBC) are not relevant for the data presented here owing to extremely low rBC concentrations. The HR-ToF-AMS was operated in "V-mode" with a mass range of $\mathrm{m/z}$ 3 – 250, alternating between ensemble mass spectrum (MS) mode for 20 s (two cycles of 5 (s) MS open and 5 (s) MS closed) and efficient particle time-of-flight (epToF) mode for 10 s. Filtered ambient air was sampled with the HR-ToF-AMS approximately three times per flight, for a duration of at least five minutes, to account for contributions from air signals. Data were analysed using the Igor Pro-based analysis tool PIKA (v.1.16) and SQUIRREL (v.1.57) (Seuper, 2010).

The HR-ToF-AMS sampled behind a pressure-controlled inlet (PCI) system, similar to that described by Hayden et al. (2011), in order to remove variations in particle sizing, transmission and air-beam signals (used to correct particle signals for variations in instrument sensitivity (Allan et al., 2003)) as a function of pressure in the aerodynamic lens (Bahreini et al., 2008; DeCarlo et al., 2008). The PCI system maintained a pressure of 6.19x10^4 Pa upstream of a 130 $\mathrm{\mu m}$ orifice in the HR-ToF-AMS inlet and downstream from a 200 $\mathrm{\mu m}$ orifice, such that the pressure in the aerodynamic lens was maintained at 173 Pa ($\sim$1.3 Torr) by variable pumping. In this configuration, the lens pressure was adequately maintained up to an altitude of $\sim$3500 m. Characterization of particle transmission efficiency with and without the PCI was carried out before and after the study (Section 1.1 in the Supplement). Results demonstrated near 100% transmission of ammonium nitrate particles from $\sim$70 – 700 nm (mobility diameter) through the PCI, by comparison to transmission through the aerodynamic lens alone (Figure S1 in the Supplement). Note that the size range over which AMS lens transmission is optimal can be very instrument dependent. HR-ToF-AMS particulate mass loadings are corrected to reflect ambient pressure, based on the AIMMS measured pressure and the PCI internal pressure.

Species comprising non-refractory particulate matter are measured with the HR-ToF-AMS, including sulfate, nitrate, ammonium and the sum of organic species, with an uncertainty of $\pm 30\%$ (Bahreini et al., 2009). The HR-ToF-AMS is capable of detecting other species, including methanesulfonic acid (Phinney et al., 2006; Zorn et al., 2008) and sea salt (Ovadnevaite et al., 2012).

The detection efficiency of sea salt containing particles is dependent on not only the ambient relative humidity, but also the temperature of the tungsten vaporizer (Ovadnevaite et al., 2012). The vaporizer temperature was calibrated with sodium nitrate particles, such that particle-time-of-flight signals indicated efficient vaporization, and was operated at a temperature of $\sim$650 $^{\circ}\mathrm{C}$. HR-ToF-AMS signals for sea salt, in particular $\mathrm{NaCl^+}$ ($\mathrm{m/z}$ 57.96), can be used to quantify sea salt mass loadings (e.g., Ovadnevaite et al., 2012); however, here we use the $\mathrm{NaCl^+}$ signal only as a qualitative indication for the presence of sea salt.

After the method of Zorn et al. (2008), we determined the fragmentation pattern for methanesulfonic acid (MSA) under the operating conditions of our HR-ToF-AMS by utilizing the unique MSA fragment $\mathrm{CH_3SO_2^+}$ ($\mathrm{m/z}$ 78.99), which was well resolved from organic fragments at the same nominal mass (i.e., $\mathrm{C_6H_7^+}$ at $\mathrm{m/z}$ 79.05, Figure S2 in the Supplement). The default HR-ToF-AMS fragmentation table was modified to include MSA, such that contributions from MSA to peaks usually associated with organic species and sulfate were accounted for. The sensitivity of our HR-ToF-AMS to MSA relative to nitrate ($\mathrm{RIE_{MSA}}$) was determined to be 1.33 ± 0.05, which is similar to estimated values used in other studies (e.g., Zorn et al., 2008). The MSA calibration and fragmentation pattern are described in more detail in Section 1.1 of the Supplement.

Ammonium nitrate calibrations (with 300 nm particles) were carried out four times during the campaign (Jimenez et al., 2003), and air-beam corrections were referenced to the appropriate calibration in order to account for differences in instrument sensitivity between flights. The relative ionization efficiencies for sulfate and ammonium ($\mathrm{RIE_{SO_4}}$ and $\mathrm{RIE_{NH_4}}$) were 1.4 ± 0.1 and 3.7 ± 0.3. The default relative ionization efficiency for organic species (i.e., $\mathrm{RIE_{Org}}$ = 1.4) was used (Jimenez et al., 2003), which may lead to some larger uncertainty in the quantification of organic aerosol mass (Murphy, 2015). Elemental composition was calculated using the method presented in Canagaratna et al. (2015). Detection limits for sulfate, nitrate, ammonium, MSA and organics based on three-times the signal-to-noise of filter measurements in flight were 0.009, 0.008, 0.004, 0.005 and 0.08 $\mathrm{\mu g\,m^{-3}}$, respectively. A composition dependent collection efficiency (CDCE) was applied to correct HR-ToF-AMS mass loadings for non-unity particle detection due to particle bounce on the tungsten vaporizer (Middlebrook et al., 2012). After the CDCE correction HR-ToF-AMS total mass loadings agreed with estimated mass concentrations from the UHSAS within a factor of two.

2.6.3 Aircraft-based Laser Ablation Aerosol Mass Spectrometer

Single particle analysis was conducted using the Aircraft-based Laser Ablation Aerosol Mass Spectrometer (ALABAMA). A detailed description of the instrument can be found in Brands et al. (2011). Briefly, the ALABAMA samples particles through a pressure-controlled inlet and an aerodynamic lens. The particles are detected and sized by light scattering when passing two continuous laser beams separated along the path of the sampled aerosol. Particle ablation and ionization is done by a single 266 nm laser pulse, and the resulting ions are detected in a bipolar time-of-flight mass spectrometer. Optical detection of aerosol limits the minimum detectable particle size to approximately 150 nm ~~, and~~ with particles at approximately 400 nm detected at the highest efficiency. The transmission efficiency in the aerodynamic lens limits the maximum detectable size to approximately 1000 nm. Particle mass spectra collected by the ALABAMA are analysed using a software package that includes *m/z* calibration, peak area integration and automated clustering using fuzzy c-means clustering (Hinz et al., 1999; Roth et al., 2016). As is done in this case study, subsets of particles can also be analysed manually by searching for selected marker peaks known from reference laboratory and field data.

A subset of ~~particles~~ 68 particles detected over the period relevant to this case study was analysed manually using marker peaks as follows. Organic carbon (OC) was characterized by peaks at $\mathrm{m/z}$ 27, 37 and 43 ($\mathrm{C_2H_3^+}$, $\mathrm{C_3H^+}$ and $\mathrm{CH_3CO^+}$ or $\mathrm{C_3H_7^+}$). Pronounced peaks at $\mathrm{m/z}$ multiples of 12 (e.g., 12, 24, ..., 108) ($\mathrm{C_n^{+/-}}$) identify elemental carbon (EC). Mass spectra containing peaks at $\mathrm{m/z}$ multiples of 12, but not higher than 36 can be either fragments of elemental or organic carbon and are therefore designated here as EC/OC. Methanesulfonic acid (MSA) was identified by a peak at $\mathrm{m/z}$ 95 ($\mathrm{CH_3SO_3^-}$). Interference from $\mathrm{Na^{37}Cl_2^-}$ is unlikely if no m/z 93 ($\mathrm{Na^{35}Cl_2^+}$) is present. Further marker peaks include $\mathrm{m/z}$ 97 ($\mathrm{HSO_4^-}$) for sulfate (S), $\mathrm{m/z}$ 26 and 42 for $\mathrm{CN^-}$ and $\mathrm{CNO^-}$ (CN), $\mathrm{m/z}$ 39 and 41 ($\mathrm{K^+}$) for potassium (K), and $\mathrm{m/z}$ 40, 56 and 57 ($\mathrm{Ca^+}$, $\mathrm{CaO^+}$, $\mathrm{CaOH^+}$) for calcium (Ca). The presence of sodium chloride (NaCl) was determined by peaks at $\mathrm{m/z}$ 23, 35, 37, 81 and 83 ($\mathrm{Na^+}$, $\mathrm{Cl^-}$ and $\mathrm{Na_2Cl^+}$). Due to chemical aging processes, $\mathrm{Cl^-}$ can be replaced by nitrate resulting in the presence of peaks at $\mathrm{m/z}$ 46 and 62 ($\mathrm{NO_2^-}$ and $\mathrm{NO_3^-}$) in addition to sodium chloride. Trimethylamine (TMA) was identified by peaks at $\mathrm{m/z}$ 58 and 59 ($\mathrm{C_3H_8N^+}$ and $\mathrm{C_3H_9N^+}$) based on laboratory reference measurements of TMA particles and previously published field data (e.g., Rehbein et al., 2011; Healy et al., 2015).

2.7 Identifying airmass history using FLEXPART-WRF

The Lagrangian particle dispersion model *FLEXible PARTicle dispersion model driven by meteorology from the* Weather Research and Forecasting model (FLEXPART-WRF) (Brioude et al., 2013) (website: flexpart.eu/wiki/FpLimitedareaWrf) was used to study the history air masses prior to sampling during the flight. FLEXPART-WRF is based on FLEXPART (Stohl et al., 2005), but uses the limited area meteorological forecast from WRF (Skamarock et al., 2001), with the specific WRF forecast details for the NETCARE campaign provided in Wentworth et al. (2015). Here, we use FLEXPART-WRF run in backward mode to study the origin of air influencing aircraft-based aerosol measurements. Further details of the FLEXPART-WRF simulations performed for NETCARE 2014 summer campaign are also found in Wentworth et al. (2015).

3 Results and Discussion

3.1 Flight overview and meteorological situation

In this case study we focus on the flight conducted on 12 July 2014 where Polar 6 travelled at $\sim$3 km altitude from Resolute Bay, past the marginal ice zone and out over open water to the eastern end of Lancaster Sound (Figure 2a) as far as was permitted by our aircraft range, at which point it descended and returned west. The relevant portion of this flight, over open water in Lancaster Sound, is highlighted in Figure 2a (79.7° W to 86.5° W, 20:00 – 21:20 UTC). During this time the aircraft flew to the west ~~at~~ below 100 m a.g.l. and covered a distance of approximately ~~200~~175 km at a survey speed of 75 $\mathrm{m\,s^{-1}}$ under clear sky conditions. Profiles were carried out at three different locations to characterize the vertical structure of the troposphere (Figure 2a, triangles): one profile from 60 m to 3000 m near Resolute Bay ($\sim$95° W, denoted as "west" in Figure 2b and c); a second, shallower profile to $\sim$900 m near the marginal ice zone ($\sim$88° W, "central"); and a third profile down from 3000 m to 60 m in eastern Lancaster Sound ($\sim$80° W,"east").

Meteorological observations and measurements of trace gases and black carbon indicate a stable and clean atmosphere. Temperature profiles in all three locations indicated a shallow surface-based temperature inversion of 2 – 4 °C, reaching up to $\sim$800 m over the ice near Resolute Bay, and to only $\sim$100 m in the eastern profile (Figure 2b). Applying the method of bulk Richardson number (Aliabadi et al., 2016a) with Polar 6 meteorological observations, and radiosondes conducted concurrently at Resolute Bay and aboard the CCGS Amundsen, Aliabadi et al. (2016b) estimated boundary layer heights of 275 ± 164 m during the NETCARE summer campaign. Here, we will refer to the portion of the boundary layer with a positive vertical gradient in the temperature profile as the "lower boundary layer." Both within and above the lower boundary layer winds were predominantly from the west, with measured wind speeds near the surface averaging 6.5±1.8 $\mathrm{m\,s^{-1}}$. Similarly, surface winds from WRF indicate predominately west-north-west winds at this time, with wind speeds of 4 – 8 $\mathrm{m\,s^{-1}}$ (Figure S4 in the Supplement). CO profiles in all three locations demonstrated very clean background conditions with concentrations ranging from 73 to 78 $\mathrm{ppb_v}$, and little variation with altitude (Figure 2c). Relative humidity was generally high near the surface, with an average of 80% in the lower boundary layer (Figure S5 in the Supplement). Refractory black carbon (rBC) concentrations also indicate a very clean atmosphere, well below the ~~thresholds~~ threshold for a clean marine boundary layer discussed by Gantt and Meskhidze (2013). Average (± standard deviation) rBC mass loadings during the period of interest and over the entire flight were $1.6 \pm 0.9\,\mathrm{ng\,m^{-3}}$ and $2.5 \pm 1.5\,\mathrm{ng\,m^{-3}}$, respectively, with slightly higher concentrations found aloft.

Air mass history from FLEXPART-WRF indicates a strong local Arctic influence on the sampled air mass. FLEXPART-WRF air mass origin is shown as the column integrated air mass residence time prior to sampling, also referred to as the column integrated potential emission sensitivity (PES), for the release time and location of this case study (Figure 3a). The column integrated PES supports that the locally-influenced air mass originated from generally clean conditions with no pollution sources. The air mass encountered by the aircraft at 82.2° W and ~85 m a.g.l. resided over ~~Devon Island~~ a snow and ice-covered island (Devon Island, (Friedl et al., 2010)) for approximately one week before descending into Lancaster Sound within one day of sampling (Figure 3). The model also indicates that the sampled air mass had a residence time within the lowest 300 m of four to five hours prior to sampling, providing at least four hours of transport and chemistry within the boundary layer (Figure 3b and c). Overall, FLEXPART-WRF air mass history suggests that the sampled air mass had little exposure to fresh sea emissions until four to five hours prior to sampling~~when it~~, when it moved from above the snow and ice covered land and was exposed to the ocean surface within the lower boundary layer.

3.2 Observations of particle growth

Our observations of particle number concentration, over the size range from 5 nm to 1 µm, indicated the simultaneous presence of nucleation mode and Aitken mode particles near the ocean surface. At low altitude near 85° W we observed an enhancement in N_{5-20} above background levels, indicating the presence ~~on~~ of nucleation mode particles (Figure 1,4a). Upon entering the lower boundary layer further downwind (Figure 2d) and to the east (82.5 – 81° W), we observed a sharp increase in N_{5-20} concurrently with an increase in N_{20-100} (Figure 4a). We do not directly observe the formation of the smallest particles; however, we hypothesize that they were formed through nucleation in a very clean atmosphere.

Particle number size distributions from 20 – 1000 nm illustrate that particles below 20 nm (Figure 4~~b~~a,c) grow to form a mode centred at 30 – 40 nm (Figure 4~~c–e~~d–f). Beyond 86° W we observe N_{20-100} at background levels of $\sim 100\,\mathrm{cm^{-3}}$. ~~We do not directly observe the formation of the smallest particles; however, we hypothesize that they were formed through nucleation in a very clean atmosphere.~~ These observations suggest that the aerosol size distribution develops as the airmass moves downwind to the east. The advection time scale from 85.8 – 81.1° W is 6.7 hr, given an average wind speed of 6.5 $\mathrm{m\,s^{-1}}$, and the sampling time of the aircraft over this distance is 35 min. Given the substantial changes in aerosol size and number concentration observed over this relatively short time period, our observations suggest that a source of condensible material contributing to aerosol growth is present to the west of the sampling region and it is unlikely that a wider source region contributed. An estimate of the growth rate in this case is associated with a large uncertainty since it is complicated by a number of factors, including the one-minute time resolution of the SMS that corresponds to a sampling distance of $\sim$4 km, and uncertainties in the advection time. Therefore, it is difficult to quantitatively follow the evolution of the size distribution. Compounded by our lack of knowledge of the spatial uniformity of the condensible material, we do not present an estimate of the growth rate here.

The boundary layer was characterized by a low pre-existing aerosol surface area (i.e., a small condensation sink). A small number of particles above 200 nm in diameter ($\sim$10 – 15 $\mathrm{cm^{-3}}$) were present within the lower boundary layer, and show a time variation distinct from that of $N_{>50}$ and $N_{>100}$ (Figure ~~??a~~4b). These larger particles are present during both sampling periods within the lower boundary layer (i.e., near 85° W and 82.5° W), where winds speeds were relatively constant (6.5$\pm$1.8 $\mathrm{m\,s^{-1}}$), and could be from ejection of primary sea-spray aerosol (see below). The small $N_{>200}$ provides a low pre-existing aerosol surface area (average $\pm$ standard deviation: 3.8$\pm$2.0 $\mathrm{\mu m^2\,cm^{-3}}$), which assists particle nucleation.

$N_{>50}$ and $N_{>100}$ show a time variation distinct from that of the nucleation mode (N_{5-20}) and larger accumulation mode particles ($N_{>200}$) (Figure 4b). In our eastern-most observations within the lower boundary layer (82.5 – 81° W) $N_{>50}$, which is accounted for largely by N_{50-150}, is enhanced above background levels of $\sim$200 $\mathrm{cm^{-3}}$ to $\sim$400 $\mathrm{cm^{-3}}$ (Figure ~~??a~~4b). At the same time, CCN concentrations are elevated to >200 $\mathrm{cm^{-3}}$, above background levels of $\sim$100 $\mathrm{cm^{-3}}$ (Figure ~~??a~~4b). $N_{>50}$, $N_{>100}$ and CCN concentrations remain somewhat elevated up to $\sim$900 m (Figure ~~??a~~4b, near 80.5° W), suggesting that some mixing above the lower boundary layer ~~is taking place to the east (profiles~~ occurred during some time prior to our observations, possibly due to katabatic winds off Devon Island suggested from the Flexpart analyses (Figure 3c). Profiles of aerosol number and composition are presented in Figure S5 in the Supplement~~)~~.

The variation in the size distribution from west to east in Lancaster Sound suggests that particles between $\sim$30 nm to greater than $\sim$50 nm are forming through secondary processes. In our western-most observations in the lower boundary layer (85.6 – 84.4° W) the size distribution is dominated by particles below 20 nm (Figure 4a,~~b~~c). Further to the east in the lower boundary layer (82.5 – 81° W) N_{5-20} is high and subsequently decreases moving east (Figure 4a), while $N_{>50}$ and $N_{>100}$ do not increase until 81.9° W (Figure ~~??a~~4b). The aircraft covered a distance of 19 km between entering the lower boundary layer (82.5° W) and observing this increase in $N_{>50}$ and $N_{>100}$. With a wind speed of 6.5 $\mathrm{m\,s^{-1}}$ near the surface, the ~~flushing time~~ advection time over this distance is approximately 50 ~~minutes~~min. If the aerosol size distribution was dominated by primary sea-spray aerosol, given constant wind speed, there would be no reason for such a delay in our observations of $N_{>50}$ and $N_{>100}$. Indeed, given the decreasing abundance of $N_{>300}$, the evidence suggests that the sea spray source, which is associated with larger particles (see below), is becoming less important as $N_{>50}$ is increasing. These observations are suggestive of a secondary process growing particles from less than 20 nm into larger sizes, above 50 nm.

3.3 Aerosol composition

3.3.1 Carbonaceous aerosol

Our observations of particle growth are correlated with an increase in organic aerosol (OA) and methanesulfonic acid (MSA) in sub-micron particles (Figure ~~??b~~5a), corresponding to increased organic-to-sulfate and MSA-to-sulfate ratios (Figure ~~??~~5b). The presence of MSA, an intermediate-volatility oxidation product of dimethylsulphide (DMS), indicates a marine-biogenic influence on the aerosol sulfur (Bates et al., 1992). MSA cannot be viewed as a conservative tracer of DMS oxidation (e.g., Bates et al., 1992); however, it is notable that the MSA-to-sulfate ratio reached a peak value of 0.15 during the growth event (corresponding to a peak mass of 60 $\mathrm{ng\,m^{-3}}$), which is significantly higher than at all other times during this flight (Figure ~~??~~5b). The absolute MSA concentration measured by the HR-ToF-AMS should be viewed as a lower limit since a portion of the MSA mass could reside on particles smaller than the lower size-limit of the instrument. Particle-size-resolved mass spectra (pToF, Figure S6 in the Supplement) during particle growth indicate that total organic aerosol was present in relatively small particle sizes, from less than 80 nm to approximately 200 nm (vacuum aerodynamic diameter, $\mathrm{d_{va}}$). Unfortunately, signal-to-noise ratios for MSA were such that little useful information could be drawn from the corresponding pToF data. The correlation of OA and MSA with particle growth suggests that the growth of particles into the size range of the HR-ToF-AMS was mediated by the condensation of MSA and condensible organic species. The source and identity of these species, aside from MSA, is not known, but we hypothesize a role for marine-derived biogenic volatile organic compounds (VOCs).

While non-marine sources of condensible organic species, such as emissions of isoprene and terpenes from high Arctic terrestrial vegetation (Schollert et al., 2014) and photochemical production of VOCs in the snowpack (Grannas et al., 2007) ~~, may~~ (e.g., over the snow and ice-covered Devon Island), could also contribute to particle growth, single particle observations of aerosol composition further suggest a marine influence on particles greater than $\sim$150 nm ($\mathrm{d_{va}}$). Fifty-four percent of particles detected by the ALABAMA over the region highlighted in Figure 2a contained detectable signal for trimethylamine (TMA, Figure 6), in support of aerosol growth through the condensation of marine-derived biogenic VOCs (e.g., Facchini et al., 2008a; Dall'Osto et al., 2012). Consistent with HR-ToF-AMS observations of MSA during the growth event, $\sim$30% of particles detected by the ALABAMA contained observable MSA signal. TMA was mainly present as an internal mixture with potassium, sulfate, other organic species and to a lesser degree with MSA (Figure 6).

Organic aerosol observed by the HR-ToF-AMS during particle growth appears chemically distinct from the OA observed at other times during this flight, especially compared to that above the lower boundary layer (OA mass spectra are presented in Figure S7 of the Supplement). Hydrocarbon fragments ($\mathrm{C_xH_y^+}$, largely unsaturated) contribute 50% to growth event OA mass spectra, and only 30% to non-growth event OA. Oxygenated organic fragments ($\mathrm{C_xH_yO_z^+}$) contribute 50% to growth event

OA mass spectra, and 70% to non-growth event OA. $C_xH_y^+$ and $C_xH_yO_z^+$ fragments are correlated during the growth event, suggesting that these less-oxygenated and more-oxygenated species are arising from a similar source. Average elemental composition also shows notable differences with oxygen-to-carbon (O:C) and hydrogen-to-carbon (H:C) ratios in the growth event OA of 0.5 and 1.6 while non-growth event OA was significantly more oxygenated with O:C and H:C ratios of 0.78 and 1.2, suggesting less aged OA during the growth event compared to other times.

To gain further insight into the characteristics of the OA observed during the growth event, we compared our mass spectrum with a number of OA mass spectra obtained with AMS instruments. The growth event OA compares favourably with marine-like OA observed at Mace Head, Ireland (R^2 = 0.75) (Ovadnevaite et al., 2011) as well as with marine OA observed over the Arctic Ocean (R^2 = 0.88) (Chang et al., 2011a). OA from the growth event also compares favourably with alpha-pinene secondary organic aerosol (SOA) generated under low NO_x conditions (R^2 = 0.78) (Chhabra et al., 2011) and with spectra associated with isoprene SOA from a forested site (R^2 = 0.85) (Robinson et al., 2011), but does not compare well with IEPOX SOA (R^2 = 0.07) (Bougiatioti et al., 2013). In conjunction with the presence of MSA during the growth event, the comparisons with previously observed marine-OA spectra support the hypothesis that we observe a marine-influenced aerosol. The comparisons with terpene-related OA could also support a marine-influenced aerosol (e.g., Shaw et al., 2010), but could also be consistent with other regional sources of these OA precursors (e.g., Grannas et al., 2007; Schollert et al., 2014).

3.3.2 Other aerosol chemical species

Other aerosol components detected by the HR-ToF-AMS showed a time variation distinct from organic aerosol species. Sulfate mass loading was relatively constant, within the lower boundary layer (Figure ~~??b~~5a), suggesting that it did not contribute significantly to particle growth during this event. Owing to the relatively slower oxidation of sulfur dioxide to sulfuric acid, it is feasible that MSA resulting from DMS oxidation could be contributing to particle growth while sulfate salts are not. However, this would be inconsistent with the results of Giamarelou et al. (2016). Similarly to the observed OA, sulfate was present in relatively small particles with a peak in the size distribution slightly larger than that of OA (Figure S6 in the Supplement). Ammonium concentrations are low and ~~not only mirror the time variation of MSA and OA during growth, but also the smooth decrease in sulfate from west to east suggesting that both organic and inorganic species~~ show some correlation with organic and inorganic aerosol species, suggesting that OA, MSA and sulfate could be partially neutralized by ammonium. The HR-ToF-AMS estimate of aerosol neutralization (accounting for sulfate, nitrate and MSA) peaks at a value of ~0.6 during particle growth (Figure ~~??~~5b).

Exclusively within the lower boundary layer we observe an increase in iodine signal as I^+ (m/z 126.90), while no other iodine-containing peaks were observed above mass spectral noise (Figure ~~??~~5c). Our observations are potentially consistent with those of Allan et al. (2015), who used similar measurements to highlight the possible role of iodine-oxide species in particle nucleation in Arctic regions. Here, I^+ shows a modest correlation not only with N_{5-20} but also with $N_{>200}$, since particles in both size ranges are confined to the lower boundary layer and their variability in time is largely dictated by the aircraft's position (Figure S8 in the Supplement). Without further information about the chemical form of the iodine we observe, it is difficult to discern whether the HR-ToF-AMS I^+ arises from iodine-oxides present in small particles or from biological iodine-containing compounds and iodine-containing salts potentially present in primary sea-spray aerosol (e.g., Murphy et al., 1997).

Primary sea spray aerosol was confined to the lower boundary layer and contributed largely to $N_{>200}$. The HR-ToF-AMS signal for $NaCl^+$, qualitatively indicating the presence of sea salt aerosol, is present in the lower boundary layer (Figure ~~??~~5c and S5 in the Supplement) and correlates well with $N_{>200}$ and $N_{>300}$ (Figure S8 in the Supplement). As mentioned above, the negative relationship between $N_{>50}$ and both $N_{>300}$ and $NaCl^+$ near 82.5° W suggests a decreasing importance of primary sea spray at the point where the secondary formation is maximum. Consistent with this observation, single particle measurements from the ALABAMA indicate that $NaCl$-containing particles were present at larger sizes (i.e., peaking at 400 nm d_{va}) and, notably, were externally mixed from other particle types containing TMA (Figure 6).

3.4 Cloud condensation nuclei (CCN)

CCN concentrations are elevated above background levels during the growth event, and are well-correlated with the number of particles greater than 80 nm ($N_{>80}$, Figure 7). If the particles contributing to CCN concentrations at this time were only composed of ammonium sulfate, under our experimental conditions (i.e., 0.6% supersaturation), we would expect the CCN-activation diameter to be $\sim$40 nm (Petters and Kreidenweis, 2007). A CCN-activation diameter of approximately 80 nm therefore indicates that a species less hygroscopic than ammonium sulfate is contributing to the CCN we observe. This is consistent with the elevated OA mass loading we measure when CCN concentrations are high (Figure 7, colour scale), while sulfate was relatively low compared to other time periods (Figure 7, marker size).

Since the aerosol was not actively dried and the supersaturation was held constant in the CCNC, in order to allow for rapid measurements, a calculation of the effective aerosol hygroscopicity parameter (κ) in this case carries a large uncertainty (Petters and Kreidenweis, 2007). In particular, measured particle diameters may be slightly larger than the corresponding dry diameter. The temperature in the inlet line was 10 – 15 $^\circ C$ warmer than the ambient temperature so that the relative humidity (RH) decreased significantly as the aerosol entered the sampling line (i.e., during the case study period, the ambient RH was 80% at 8 – 10 $^\circ C$, and the RH decreased within the inlet to approximately $<$ 30%). Using the measured aerosol composition, we estimate that measured particle diameters are up to 10% larger than the corresponding dry diameter.

Nonetheless, this calculation is still illustrative of the organic aerosol properties in this environment. If the kappa value of the organic aerosol (κ_{Org}) is 0.1, and κ for the whole aerosol is calculated based on the HR-ToF-AMS organic and sulfate loadings and the known κ for ammonium sulfate, then the resulting dry diameter for activation is $\sim$60 nm. From our measurements, the activation diameter seems to be larger than 60 nm so that κ_{Org} of 0.1 could be regarded as an upper limit. If we overestimate aerosol size by 10%, due to incomplete drying in our sampling line, then our estimated CCN-activation diameter and the calculated dry diameter for activation become more similar. Overall, this illustrates that the organic aerosol was relatively non-hygroscopic with $\kappa_{\mathrm{Org}} \sim 0.1$. This estimate is within the range of κ_{Org} recently measured in a coastal, marine influenced environment by Yakobi-Hancock et al. (2014).

4 Conclusions

In this case study, we present evidence that growth of nucleation mode particles in the summertime Arctic can be mediated by the condensation of methanesulfonic acid (MSA) and condensible organic species. Our observations of particle growth, informed by observations of particle composition, suggest a combination of primary and secondary aerosol across the size distribution. We observe the growth of small particles, less than 20 nm, into sizes above 50 nm, while our measurements suggest that ejection of primary sea-spray aerosol contributes to externally mixed particles larger than 200 nm. The small $\mathrm{N}_{>200}$, that are likely from direct emissions of sea-spray, could contain a substantial fraction of organic aerosol (OA). However, the majority of OA mass observed here is best correlated with MSA, $\mathrm{N}_{>80}$ (dominated by N_{80-150}), and the presence of trimethylamine (TMA) suggesting that this OA is largely secondary in origin. As well, it occurs simultaneously with a period of pronounced aerosol growth. Together, this indicates that the cloud condensation nuclei (CCN) we observe are largely controlled by secondary processes.

Very few studies have measured aerosol composition at high time resolution in the summertime Arctic. Even fewer studies have provided evidence for secondary organic aerosol formation in Arctic regions, in part owing to the infrequency of measurements in the remote marine boundary layer. These results highlight the potential importance of secondary marine organic aerosol formation, and its role in growing nucleation mode particles into CCN-active sizes in the clean summertime Arctic atmosphere. Future measurements of nucleation and Aitken mode particle composition coupled to characterization of gas-phase organic species will greatly improve our understanding of particle formation and growth in remote regions, aiding in our ability to understand resulting aerosol-cloud-climate interactions.

Acknowledgements. The authors thank Kenn Borek Air Ltd., in particular our pilots Kevin Elke and John Bayes, as well as our aircraft maintenance engineer Kevin Riehl. We gratefully acknowledge John Ford and

David Heath at the University of Toronto Chemistry machine shop for their work racking the HR-ToF-AMS and other instruments for deployment aboard Polar 6. We are grateful to Katherine Hayden (Environment and Climate Change Canada, ECCC) for loaning us the pressure controlled inlet used with the HR-ToF-AMS. We thank Jim Hodgson and Lake Central Air Services in Muskoka, Jim Watson (Scale Modelbuilders, Inc.), Julia Binder and Martin Gerhmann (Alfred Wegener Institute, AWI), Mike Harwood and Andrew Elford (ECCC), for their support of the integration of the instrumentation in the aircraft. We thank Carrie Taylor (ECCC), Bob Christensen (UofT), Lukas Kandora, Manuel Sellmann and Jens Herrmann (AWI), Desiree Toom, Sangeeta Sharma, Dan Veber, Andrew Platt, Anne Marie Macdonald, Ralf Staebler, Maurice Watt (ECCC) and Kathy Law (LATMOS) for their support before and during the study. We thank the Biogeochemistry department of MPIC for providing the CO instrument and Dieter Scharffe for his support during the preparation phase of the campaign. We thank the Nunavut Research Institute and the Nunavut Impact Review Board for licensing the study. Logistical support in Resolute Bay was provided by the Polar Continental Shelf Project (PCSP) of Natural Resources Canada under PCSP Field Project 218-14, and we are particularly grateful to Tim McCagherty and Jodi MacGregor of the PCSP. Funding for this work was provided by the Natural Sciences and Engineering Research Council of Canada through the NETCARE project of the Climate Change and Atmospheric Research Program, the Alfred Wegener Institute and Environment and Climate Change Canada.

References

Aliabadi, A. A., Staebler, R., de Grandpré, J., Zadra, A., and Vaillancourt, P.: Comparison of estimated atmospheric boundary layer mixing height in the Arctic and Southern Great Plains under statically stable conditions: Experimental and numerical aspects, Atmos. Ocean, doi:10.1080/07055900.2015.1119100, 2016a.

Aliabadi, A. A., Staebler, R., Liu, M., and Herber, A.: Characterization and parameterization of Reynolds stress and turbulent heat flux in the stably-stratified lower Arctic troposphere using aircraft measurements, Boundary-Layer Meteorology, in Press, 2016b.

Allan, J. D., Alfarra, M. R., Bower, K. N., Williams, P. I., Gallagher, M. W., Jimenez, J. L., McDonald, A. G., Nemitz, E., Canagaratna, M. R., Jayne, J. T., Coe, H., and Worsnop, D. R.: Quantitative sampling using an Aerodyne aerosol mass spectrometer 2. Measurements of fine particulate chemical composition in two U.K. cities, Journal of Geophysical Research: Atmospheres, 108, doi:10.1029/2002JD002359, 4091, 2003.

Allan, J. D., Williams, P. I., Najera, J., Whitehead, J. D., Flynn, M. J., Taylor, J. W., Liu, D., Darbyshire, E., Carpenter, L. J., Chance, R., Andrews, S. J., Hackenberg, S. C., and McFiggans, G.: Iodine observed in new particle formation events in the Arctic atmosphere during ACCACIA, Atmospheric Chemistry and Physics, 15, 5599–5609, 2015.

Almeida, J., Schobesberger, S., Kurten, A., Ortega, I. K., Kupiainen-Maatta, O., Praplan, A. P., Adamov, A., Amorim, A., Bianchi, F., Breitenlechner, M., David, A., Dommen, J., Donahue, N. M., Downard, A., Dunne, E., Duplissy, J., Ehrhart, S., Flagan, R. C., Franchin, A., Guida, R., Hakala, J., Hansel, A., Heinritzi, M., Henschel, H., Jokinen, T., Junninen, H., Kajos, M., Kangasluoma, J., Keskinen, H., Kupc, A., Kurten, T., Kvashin, A. N., Laaksonen, A., Lehtipalo, K., Leiminger, M., Leppa, J., Loukonen, V., Makhmutov, V., Mathot, S., McGrath, M. J., Nieminen, T., Olenius, T., Onnela, A., Petaja, T., Riccobono, F., Riipinen, I., Rissanen, M., Rondo, L., Ruuskanen, T., Santos, F. D., Sarnela, N., Schallhart, S., Schnitzhofer, R., Seinfeld, J. H., Simon, M., Sipila, M., Stozhkov, Y., Stratmann, F., Tome, A., Trostl, J., Tsagkogeorgas, G., Vaattovaara, P., Viisanen, Y., Virtanen, A., Vrtala, A., Wagner, P. E., Weingartner, E., Wex, H., Williamson, C., Wimmer, D., Ye, P., Yli-Juuti, T., Carslaw, K. S., Kulmala, M., Curtius, J., Baltensperger, U., Worsnop, D. R., Vehkamaki, H., and Kirkby, J.: Molecular understanding of sulphuric acid-amine particle nucleation in the atmosphere, Nature, 502, 359–363, http://dx.doi.org/10.1038/nature12663, 2013.

Bahreini, R., Dunlea, E. J., Matthew, B. M., Simons, C., Docherty, K. S., DeCarlo, P. F., Jimenez, J. L., Brock, C. A., and Middlebrook, A. M.: Design and Operation of a Pressure-Controlled Inlet for Airborne Sampling with an Aerodynamic Aerosol Lens, Aerosol Science and Technology, 42, 465–471, doi:10.1080/02786820802178514, 2008.

Bahreini, R., Ervens, B., Middlebrook, A. M., Warneke, C., de Gouw, J. A., DeCarlo, P. F., Jimenez, J. L., Brock, C. A., Neuman, J. A., Ryerson, T. B., Stark, H., Atlas, E., Brioude, J., Fried, A., Holloway, J. S., Peischl, J., Richter, D., Walega, J., Weibring, P., Wollny, A. G., and Fehsenfeld, F. C.: Organic aerosol formation in urban and industrial plumes near Houston and Dallas, Texas, Journal of Geophysical Research: Atmospheres, 114, doi:10.1029/2008JD011493, http://dx.doi.org/10.1029/2008JD011493, D00F16, 2009.

Bates, T. S., Calhoun, J. A., and Quinn, P. K.: Variations in the methanesulfonate to sulfate molar ratio in submicrometer marine aerosol particles over the south Pacific Ocean, Journal of Geophysical Research: Atmospheres, 97, 9859–9865, doi:10.1029/92JD00411, http://dx.doi.org/10.1029/92JD00411, 1992.

Bigg, E. K. and Leck, C.: Cloud-active particles over the central Arctic Ocean, Journal of Geophysical Research: Atmospheres, 106, 32 155–32 166, doi:10.1029/1999JD901152, http://dx.doi.org/10.1029/1999JD901152, 2001.

Bougiatioti, A., Zarmpas, P., Koulouri, E., Antoniou, M., Theodosi, C., Kouvarakis, G., Saarikoski, S., Mäkelä, T., Hillamo, R., and Mihalopoulos, N.: Organic, elemental and water-soluble organic carbon in size segregated aerosols, in the marine boundary layer of the Eastern Mediterranean, Atmospheric Environment, 64, 251 – 262, doi:http://dx.doi.org/10.1016/j.atmosenv.2012.09.071, 2013.

Brands, M., Kamphus, M., Böttger, T., Schneider, J., Drewnick, F., Roth, A., Curtius, J., Voigt, C., Borbon, A., Beekmann, M., Bourdon, A., Perrin, T., and Borrmann, S.: Characterization of a Newly Developed Aircraft-Based Laser Ablation Aerosol Mass Spectrometer (ALABAMA) and First Field Deployment in Urban Pollution Plumes over Paris During MEGAPOLI 2009, Aerosol Science and Technology, 45, 46–64, doi:10.1080/02786826.2010.517813, 2011.

Brioude, J., Arnold, D., Stohl, A., Cassiani, M., Morton, D., Seibert, P., Angevine, W., Evan, S., Dingwell, A., Fast, J. D., Easter, R. C., Pisso, I., Burkhart, J., and Wotawa, G.: The Lagrangian particle dispersion model FLEXPART-WRF version 3.1, Geoscientific Model Development, 6, 1889–1904, doi:10.5194/gmd-6-1889-2013, http://www.geosci-model-dev.net/6/1889/2013/, 2013.

Browse, J., Carslaw, K. S., Mann, G. W., Birch, C. E., Arnold, S. R., and Leck, C.: The complex response of Arctic aerosol to sea-ice retreat, Atmospheric Chemistry and Physics, 14, 7543–7557, 2014.

Bzdek, B. R., Lawler, M. J., Horan, A. J., Pennington, M. R., DePalma, J. W., Zhao, J., Smith, J. N., and Johnston, M. V.: Molecular constraints on particle growth during new particle formation, Geophysical Research Letters, 41, 6045–6054, doi:10.1002/2014GL060160, http://dx.doi.org/10.1002/2014GL060160, 2014.

Cai, Y., D. C. Montague, D., Mooiweer-Bryan, W., and Deshler, T.: Performance characteristics of the ultra-high sensitivity aerosol spectrometer for particles between 55 and 800 nm: Laboratory and field studies, Journal of Aerosol Science, 39, 759–769, 2008.

Canagaratna, M. R., Jimenez, J. L., Kroll, J. H., Chen, Q., Kessler, S. H., Massoli, P., Hildebrandt Ruiz, L., Fortner, E., Williams, L. R., Wilson, K. R., Surratt, J. D., Donahue, N. M., Jayne, J. T., and Worsnop, D. R.: Elemental ratio measurements of organic compounds using aerosol mass spectrometry: characterization, improved calibration, and implications, Atmospheric Chemistry and Physics, 15, 253–272, doi:10.5194/acp-15-253-2015, http://www.atmos-chem-phys.net/15/253/2015/, 2015.

Cavalieri, D. J., Parkinson, C., Gloersen, P., and Zwally, H.: Sea Ice Concentrations from Nimbus-7 SMMR and DMSP SSM/I-SSMIS Passive Microwave Data, Boulder, Colorado USA: NASA National Snow and Ice Data Center Distributed Active Archive Center, ttp://dx.doi.org/10.5067/8GQ8LZQVL0VL, 1996.

Ceburnis, D., O'Dowd, C. D., Jennings, G. S., Facchini, M. C., Emblico, L., Decesari, S., Fuzzi, S., and Sakalys, J.: Marine aerosol chemistry gradients: Elucidating primary and secondary processes and fluxes, Geophysical Research Letters, 35, n/a–n/a, doi:10.1029/2008GL033462, http://dx.doi.org/10.1029/2008GL033462, L07804, 2008.

Chang, R. Y.-W., Slowik, J. G., Shantz, N. C., Vlasenko, A., Liggio, J., Sjostedt, S. J., Leaitch, W. R., and Abbatt, J. P. D.: The hygroscopicity parameter (kappa) of ambient organic aerosol at a field site subject to biogenic and anthropogenic influences: relationship to degree of aerosol oxidation, Atmospheric Chemistry and

Physics, 10, 5047–5064, doi:10.5194/acp-10-5047-2010, http://www.atmos-chem-phys.net/10/5047/2010/, 2010.

Chang, R. Y. W., Leck, C., Graus, M., Muller, M., Paatero, J., Burkhart, J. F., Stohl, A., Orr, L. H., Hayden, K., Li, S. M., Hansel, A., Tjernstrom, M., Leaitch, W. R., and Abbatt, J. P. D.: Aerosol composition and sources in the central Arctic Ocean during ASCOS, Atmospheric Chemistry and Physics, 11, 10 619–10 636, 2011a.

Chang, R. Y.-W., Sjostedt, S. J., Pierce, J. R., Papakyriakou, T. N., Scarratt, M. G., Michaud, S., Levasseur, M., Leaitch, W. R., and Abbatt, J. P. D.: Relating atmospheric and oceanic DMS levels to particle nucleation events in the Canadian Arctic, Journal of Geophysical Research: Atmospheres, 116, n/a–n/a, doi:10.1029/2011JD015926, http://dx.doi.org/10.1029/2011JD015926, D00S03, 2011b.

Chhabra, P. S., Ng, N. L., Canagaratna, M. R., Corrigan, A. L., Russell, L. M., Worsnop, D. R., Flagan, R. C., and Seinfeld, J. H.: Elemental composition and oxidation of chamber organic aerosol, Atmospheric Chemistry and Physics, 11, 8827–8845, doi:10.5194/acp-11-8827-2011, http://www.atmos-chem-phys.net/11/8827/2011/, 2011.

Claeys, M., Wang, W., Vermeylen, R., Kourtchev, I., Chi, X., Farhat, Y., Surratt, J., Gomez-Gonzalez, Y., Sciare, J., and Maenhaut, W.: Chemical characterisation of marine aerosol at Amsterdam Island during the austral summer of 2006 - 2007, Journal of Aerosol Science, 41, 13–22, doi:10.1016/j.jaerosci.2009.08.003, 2010.

Clarke, A. D., Owens, S. R., and Zhou, J.: An ultrafine sea-salt flux from breaking waves: Implications for cloud condensation nuclei in the remote marine atmosphere, Journal of Geophysical Research: Atmospheres, 111, n/a–n/a, doi:10.1029/2005JD006565, http://dx.doi.org/10.1029/2005JD006565, D06202, 2006.

Croft, B., Martin, R. V., Leaitch, W. R., Tunved, P., Breider, T. J., D'Andrea, S. D., and Pierce, J. R.: Processes controlling the seasonal cycle of Arctic aerosol number and size distributions, Atmospheric Chemistry and Physics Discussions, 15, 29 079–29 124, doi:10.5194/acpd-15-29079-2015, http://www.atmos-chem-phys-discuss.net/15/29079/2015/, 2015.

Curry, J. A.: Interactions among aerosols, clouds and climate of the Arctic Ocean, The Science of the Total Environment, 160, 777–791, 1995.

Dall'Osto, M., Ceburnis, D., Monahan, C., Worsnop, D. R., Bialek, J., Kulmala, M., Kurtén, T., Ehn, M., Wenger, J., Sodeau, J., Healy, R., and O'Dowd, C.: Nitrogenated and aliphatic organic vapors as possible drivers for marine secondary organic aerosol growth, Journal of Geophysical Research: Atmospheres, 117, n/a–n/a, doi:10.1029/2012JD017522, http://dx.doi.org/10.1029/2012JD017522, D12311, 2012.

DeCarlo, P. F., Kimmel, J. R., Trimborn, A., Northway, M. J., Jayne, J. T., Aiken, A. C., Gonin, M., Fuhrer, K., Horvath, T., Docherty, K. S., Worsnop, D. R., and Jimenez, J. L.: Field-deployable, high-resolution, time-of-flight aerosol mass spectrometer, Analytical Chemistry, 78, 8281–8289, 2006.

DeCarlo, P. F., Dunlea, E. J., Kimmel, J. R., Aiken, A. C., Sueper, D., Crounse, J., Wennberg, P. O., Emmons, L., Shinozuka, Y., Clarke, A., Zhou, J., Tomlinson, J., Collins, D. R., Knapp, D., Weinheimer, A. J., Montzka, D. D., Campos, T., and Jimenez, J. L.: Fast airborne aerosol size and chemistry measurements above Mexico City and Central Mexico during the MILAGRO campaign, Atmospheric Chemistry and Physics, 8, 4027–4048, doi:10.5194/acp-8-4027-2008, http://www.atmos-chem-phys.net/8/4027/2008/, 2008.

Decesari, S., Finessi, E., Rinaldi, M., Paglione, M., Fuzzi, S., Stephanou, E. G., Tziaras, T., Spyros, A., Ceburnis, D., O'Dowd, C., Dall'Osto, M., Harrison, R. M., Allan, J., Coe, H., and Facchini, M. C.: Primary and secondary marine organic aerosols over the North Atlantic Ocean during the MAP experiment, Journal of

Geophysical Research: Atmospheres, 116, n/a–n/a, doi:10.1029/2011JD016204, http://dx.doi.org/10.1029/2011JD016204, D22210, 2011.

Ehn, M., Thornton, J. A., Kleist, E., Sipila, M., Junninen, H., Pullinen, I., Springer, M., Rubach, F., Tillmann, R., Lee, B., Lopez-Hilfiker, F., Andres, S., Acir, I.-H., Rissanen, M., Jokinen, T., Schobesberger, S., Kangasluoma, J., Kontkanen, J., Nieminen, T., Kurten, T., Nielsen, L. B., Jorgensen, S., Kjaergaard, H. G., Canagaratna, M., Maso, M. D., Berndt, T., Petaja, T., Wahner, A., Kerminen, V.-M., Kulmala, M., Worsnop, D. R., Wildt, J., and Mentel, T. F.: A large source of low-volatility secondary organic aerosol, Nature, 506, 476–479, http://dx.doi.org/10.1038/nature13032, 2014.

Engvall, A. C., Krejci, R., Strom, J., Treffeisen, R., Scheele, R., Hermansen, O., and Paatero, J.: Changes in aerosol properties during spring-summer period in the Arctic troposphere, Atmospheric Chemistry and Physics, 8, 445–462, 2008.

Facchini, M., Decesari, S., Rinaldi, M., Carbone, C., Finessi, E., Mihaela, M., Fuzzi, S., Moretti, F., Tagliavini, E., Ceburnis, D., and O'Dowd, C.: Important Source of Marine Secondary Organic Aerosol from Biogenic Amines, Environmental Science and Technology, 42, 9116–9121, doi:10.1021/es8018385, 2008a.

Facchini, M. C., Rinaldi, M., Decesari, S., Carbone, C., Finessi, E., Mircea, M., Fuzzi, S., Ceburnis, D., Flanagan, R., Nilsson, E. D., de Leeuw, G., Martino, M., Woeltjen, J., and O'Dowd, C. D.: Primary submicron marine aerosol dominated by insoluble organic colloids and aggregates, Geophysical Research Letters, 35, n/a–n/a, doi:10.1029/2008GL034210, http://dx.doi.org/10.1029/2008GL034210, L17814, 2008b.

Friedl, M., Sulla-Menashe, D., Tan, B., Schneider, A., Ramankutty, N., Sibley, A., and Huang, X.: MODIS Collection 5 global land cover: Algorithm refinements and characterization of new datasets, Collection 5.1 IGBP Land Cover, 2010.

Frossard, A. A., Russell, L. M., Burrows, S. M., Elliott, S. M., Bates, T. S., and Quinn, P. K.: Sources and composition of submicron organic mass in marine aerosol particles, Journal of Geophysical Research-Atmospheres, 119, 12 977–13 003, 2014.

Fu, P. Q., Kawamura, K., Chen, J., and Barrie, L. A.: Isoprene, Monoterpene, and Sesquiterpene Oxidation Products in the High Arctic Aerosols during Late Winter to Early Summer, Environmental Science and Technology, 43, 4022–4028, 2009.

Fu, P. Q., Kawamura, K., Chen, J., Charrière, B., and Sempéré, R.: Organic molecular composition of marine aerosols over the Arctic Ocean in summer: contributions of primary emission and secondary aerosol formation, Biogeosciences, 10, 653–667, doi:10.5194/bg-10-653-2013, http://www.biogeosciences.net/10/653/2013/, 2013.

Fu, P. Q., Kawamura, K., Chen, J., Qin, M., Ren, L., Sun, Y., Wang, Z., Barrie, L., Tachibana, E., Ding, A., and Yamashita, Y.: Fluorescent water-soluble organic aerosols in the High Arctic atmosphere, Scientific Reports, 5, doi:10.1038/srep09845, 2015.

Gantt, B. and Meskhidze, N.: The physical and chemical characteristics of marine primary organic aerosol: a review, Atmospheric Chemistry and Physics, 13, 3979–3996, 2013.

Gantt, B., Meskhidze, N., and Kamykowski, D.: A new physically-based quantification of marine isoprene and primary organic aerosol emissions, Atmospheric Chemistry and Physics, 9, 4915–4927, doi:10.5194/acp-9-4915-2009, http://www.atmos-chem-phys.net/9/4915/2009/, 2009.

Gao, R. S., Schwarz, J. P., Kelly, K. K., Fahey, D. W., Watts, L. A., Thompson, T. L., Spackman, J. R., Slowik, J. G., Cross, E. S., Han, J.-H., Davidovits, P., Onasch, T. B., and Worsnop, D. R.: A Novel Method for Estimating Light-Scattering Properties of Soot Aerosols Using a Modified Single-Particle Soot Photometer, Aerosol Science and Technology, 41, 125–135, doi:10.1080/02786820601118398, 2007.

Garrett, T. J., Brattström, S., Sharma, S., Worthy, D. E. J., and Novelli, P.: The role of scavenging in the seasonal transport of black carbon and sulfate to the Arctic, Geophysical Research Letters, 38, n/a–n/a, doi:10.1029/2011GL048221, http://dx.doi.org/10.1029/2011GL048221, L16805, 2011.

Giamarelou, M., Eleftheriadis, K., Nyeki, S., Tunved, P., Torseth, K., and Biskos, G.: Indirect evidence of the composition of nucleation mode atmospheric particles in the high Arctic, Journal of Geophysical Research: Atmospheres, 121, 965–975, doi:10.1002/2015JD023646, http://dx.doi.org/10.1002/2015JD023646, 2015JD023646, 2016.

Gosselin, M., Charette, J., Blais, M., Gourdal, M., Lizotte, M., Levasseur, M., Tremblay, J., and Gratton, Y.: Phytoplankton dynamics at receding ice edges in the Canadian High Arctic, http://www.netcare-project.ca/workshops/netcare-workshop-2015/, 3rd Annual NETCARE Workshop, University of Toronto, Toronto, Ontario, Canada, 2015.

Grannas, A. M., Jones, A. E., Dibb, J., Ammann, M., Anastasio, C., Beine, H. J., Bergin, M., Bottenheim, J., Boxe, C. S., Carver, G., Chen, G., Crawford, J. H., Dominé, F., Frey, M. M., Guzmán, M. I., Heard, D. E., Helmig, D., Hoffmann, M. R., Honrath, R. E., Huey, L. G., Hutterli, M., Jacobi, H. W., Klán, P., Lefer, B., McConnell, J., Plane, J., Sander, R., Savarino, J., Shepson, P. B., Simpson, W. R., Sodeau, J. R., von Glasow, R., Weller, R., Wolff, E. W., and Zhu, T.: An overview of snow photochemistry: evidence, mechanisms and impacts, Atmospheric Chemistry and Physics, 7, 4329–4373, doi:10.5194/acp-7-4329-2007, http://www.atmos-chem-phys.net/7/4329/2007/, 2007.

Hansen, A. M. K., Kristensen, K., Nguyen, Q. T., Zare, A., Cozzi, F., Nojgaard, J. K., Skov, H., Brandt, J., Christensen, J. H., Strom, J., Tunved, P., Krejci, R., and Glasius, M.: Organosulfates and organic acids in Arctic aerosols: speciation, annual variation and concentration levels, Atmospheric Chemistry and Physics, 14, 7807–7823, 2014.

Hayden, K. L., Sills, D. M. L., Brook, J. R., Li, S.-M., Makar, P. A., Markovic, M. Z., Liu, P., Anlauf, K. G., O'Brien, J. M., Li, Q., and McLaren, R.: Aircraft study of the impact of lake-breeze circulations on trace gases and particles during BAQS-Met 2007, Atmospheric Chemistry and Physics, 11, 10 173–10 192, doi:10.5194/acp-11-10173-2011, http://www.atmos-chem-phys.net/11/10173/2011/, 2011.

Healy, R. M., Evans, G. J., Murphy, M., Sierau, B., Arndt, J., McGillicuddy, E., O'Connor, I. P., Sodeau, J. R., and Wenger, J. C.: Single-particle speciation of alkylamines in ambient aerosol at five European sites, Analytical and Bioanalytical Chemistry, 407, 5899–5909, 2015.

Heintzenberg, J. and Leck, C.: The summer aerosol in the central Arctic 1991-2008: did it change or not?, Atmospheric Chemistry and Physics, 12, 3969–3983, 2012.

Heintzenberg, J., Leck, C., and Tunved, P.: Potential source regions and processes of aerosol in the summer Arctic, Atmospheric Chemistry and Physics, 15, 6487–6502, 2015.

Herber, A., Dethloff, K., Haas, C., Steinhage, D., Strapp, J. W., Bottenheim, J., McElroy, T., and Yamanouchi, T.: POLAR 5 - a new research aircraft for improved access to the Arctic, ISAR-1, Drastic Change under the Global Warming, Extended Abstract, pp. 54–57, 10013/epic.34660, 2008.

Hinz, K.-P., Greweling, M., Drews, F., and Spengler, B.: Data processing in on-line laser mass spectrometry of inorganic, organic, or biological airborne particles, Journal of the American Society for Mass Spectrometry, 10, 648 – 660, doi:http://dx.doi.org/10.1016/S1044-0305(99)00028-8, http://www.sciencedirect.com/science/article/pii/S1044030599000288, 1999.

Intrieri, J. M., Fairall, C. W., Shupe, M. D., Persson, P. O. G., Andreas, E. L., Guest, P. S., and Moritz, R. E.: An annual cycle of Arctic surface cloud forcing at SHEBA, Journal of Geophysical Research: Oceans, 107, SHE 13–1 – SHE 13–14, doi:10.1029/2000JC000439, http://dx.doi.org/10.1029/2000JC000439, 8039, 2002.

Jeffries, M. and Richter-Menge, J.: The Arctic in "State of the Climate in 2011", Bulletin of the American Meteorological Society, 93, S127–147, doi:http://dx.doi.org/10.1175/2012BAMSStateoftheClimate.1, 2012.

Jimenez, J. L., Jayne, J. T., Shi, Q., Kolb, C. E., Worsnop, D. R., Yourshaw, I., Seinfeld, J. H., Flagan, R. C., Zhang, X., Smith, K. A., Morris, J. W., and Davidovits, P.: Ambient aerosol sampling using the Aerodyne Aerosol Mass Spectrometer, Journal of Geophysical Research: Atmospheres, 108, n/a–n/a, doi:10.1029/2001JD001213, http://dx.doi.org/10.1029/2001JD001213, 8425, 2003.

Karl, M., Leck, C., Gross, A., and Pirjola, L.: A study of new particle formation in the marine boundary layer over the central Arctic Ocean using a flexible multicomponent aerosol dynamic model, Tellus B, 64, doi:10.3402/tellusb.v64i0.17158, http://www.tellusb.net/index.php/tellusb/article/view/17158, 17158, 2012.

Karl, M., Leck, C., Coz, E., and Heintzenberg, J.: Marine nanogels as a source of atmospheric nanoparticles in the high Arctic, Geophysical Research Letters, 40, 3738–3743, doi:10.1002/grl.50661, http://dx.doi.org/10.1002/grl.50661, 2013.

Kawamura, K., Ono, K., Tachibana, E., Charriere, B., and Sempere, R.: Distributions of low molecular weight dicarboxylic acids, ketoacids and alpha-dicarbonyls in the marine aerosols collected over the Arctic Ocean during late summer, Biogeosciences, 9, 4725–4737, 2012.

Kay, J. E. and Gettelman, A.: Cloud influence on and response to seasonal Arctic sea ice loss, Journal of Geophysical Research: Atmospheres, 114, n/a–n/a, doi:10.1029/2009JD011773, http://dx.doi.org/10.1029/2009JD011773, D18204, 2009.

Kopec, B. G., Feng, X., Michel, F. A., and Posmentier, E. S.: Influence of sea ice on Arctic precipitation, Proceedings of the National Academy of Sciences, 113, 46–51, doi:10.1073/pnas.1504633113, http://www.pnas.org/content/113/1/46.abstract, 2016.

Kulmala, M. and Kerminen, V.-M.: On the formation and growth of atmospheric nanoparticles, Atmospheric Research, 90, 132 – 150, doi:http://dx.doi.org/10.1016/j.atmosres.2008.01.005, http://www.sciencedirect.com/science/article/pii/S0169809508000082, 17th International Conference on Nucleation and Atmospheric Aerosols, 2008.

Laborde, M., Schnaiter, M., Linke, C., Saathoff, H., Naumann, K.-H., Möhler, O., Berlenz, S., Wagner, U., Taylor, J. W., Liu, D., Flynn, M., Allan, J. D., Coe, H., Heimerl, K., Dahlkötter, F., Weinzierl, B., Wollny, A. G., Zanatta, M., Cozic, J., Laj, P., Hitzenberger, R., Schwarz, J. P., and Gysel, M.: Single Particle Soot Photometer intercomparison at the AIDA chamber, Atmospheric Measurement Techniques, 5, 3077–3097, doi:10.5194/amt-5-3077-2012, http://www.atmos-meas-tech.net/5/3077/2012/, 2012.

Law, K. S. and Stohl, A.: Arctic air pollution: Origins and impacts, Science, 315, 1537–1540, 2007.

Lawler, M. J., Whitehead, J., O'Dowd, C., Monahan, C., McFiggans, G., and Smith, J. N.: Composition of 15-85 nm particles in marine air, Atmospheric Chemistry and Physics, 14, 11 557–11 569, doi:10.5194/acp-14-11557-2014, http://www.atmos-chem-phys.net/14/11557/2014/, 2014.

Leaitch, W. R., Sharma, S., L., H., Toom-Sauntry, D., Chivulescu, A., Macdonald, A., von Salzen, K., J.R., P., Bertram, A., C. Schroder, J., Shantz, N., Chang, R. Y.-W., and A.-L., N.: Dimethyl sulfide control of the clean summertime Arctic aerosol and cloud, Elementa, 1, doi:10.12952/journal.elementa.000017, 2013.

Leaitch, W. R., Korolev, A., Aliabadi, A. A., Burkart, J., Willis, M., Abbatt, J. P. D., Bozem, H., Hoor, P., Kollner, F., Schneider, J., Herber, A., Konrad, C., and Brauner, R.: Effects of 20-100 nanometre particles on liquid clouds in the clean summertime Arctic, Atmospheric Chemistry and Physics Discussions, 2016, 1–50, doi:10.5194/acp-2015-999, http://www.atmos-chem-phys-discuss.net/acp-2015-999/, in review, 2016.

Lindsay, R., Zhang, J., Steele, M., and Stern, H.: Arctic sea-ice retreat in 2007 follows thinning trend, Journal of Climate, 22, 165–176, doi:http://dx.doi.org/10.1175/2008JCLI2521.1, 2009.

Lubin, D. and Vogelmann, A. M.: A climatologically significant aerosol longwave indirect effect in the Arctic, Nature, 439, 453–456, 2006.

Mahajan, A. S., Shaw, M., Oetjen, H., Hornsby, K. E., Carpenter, L. J., Kaleschke, L., Tian-Kunze, X., Lee, J. D., Moller, S. J., Edwards, P., Commane, R., Ingham, T., Heard, D. E., and Plane, J. M. C.: Evidence of reactive iodine chemistry in the Arctic boundary layer, Journal of Geophysical Research: Atmospheres, 115, doi:10.1029/2009JD013665, http://dx.doi.org/10.1029/2009JD013665, D20303, 2010.

Mauritsen, T., Sedlar, J., Tjernstrom, M., Leck, C., Martin, M., Shupe, M., Sjogren, S., Sierau, B., Persson, P. O. G., Brooks, I. M., and Swietlicki, E.: An Arctic CCN-limited cloud-aerosol regime, Atmospheric Chemistry and Physics, 11, 165–173, 2011.

Metzger, A., Verheggen, B., Dommen, J., Duplissy, J., Prevot, A. S. H., Weingartner, E., Riipinen, I., Kulmala, M., Spracklen, D. V., Carslaw, K. S., and Baltensperger, U.: Evidence for the role of organics in aerosol particle formation under atmospheric conditions, Proceedings of the National Academy of Sciences, 107, 6646–6651, doi:10.1073/pnas.0911330107, http://www.pnas.org/content/107/15/6646.abstract, 2010.

Middlebrook, A. M., Bahreini, R., Jimenez, J. L., and Canagaratna, M. R.: Evaluation of Composition-Dependent Collection Efficiencies for the Aerodyne Aerosol Mass Spectrometer using Field Data, Aerosol Science and Technology, 46, 258–271, doi:10.1080/02786826.2011.620041, 2012.

Mungall, E. L., Croft, B., Lizotte, M., Thomas, J. L., Murphy, J. G., Levasseur, M., Martin, R. V., Wentzell, J. J. B., Liggio, J., and Abbatt, J. P. D.: Summertime sources of dimethyl sulfide in the Canadian Arctic Archipelago and Baffin Bay, Atmospheric Chemistry and Physics Discussions, 15, 35 547–35 589, doi:10.5194/acpd-15-35547-2015, http://www.atmos-chem-phys-discuss.net/15/35547/2015/, in reveiw, 2015.

Murphy, D. M.: The effects of molecular weight and thermal decomposition on the sensitivity of a thermal desorption aerosol mass spectrometer, Aerosol Science and Technology, 50, 118–125, doi:10.1080/02786826.2015.1136403, 2015.

Murphy, D. M., Thomson, D. S., and Middlebrook, A. M.: Bromine, iodine, and chlorine in single aerosol particles at Cape Grim, Geophysical Research Letters, 24, 3197–3200, 1997.

Narukawa, M., Kawamura, K., Li, S.-M., and Bottenheim, J. W.: Stable carbon isotopic ratios and ionic composition of the high-Arctic aerosols: An increase in delta-13C values from winter to spring, Journal of Geophysical Research: Atmospheres, 113, doi:10.1029/2007JD008755, http://dx.doi.org/10.1029/2007JD008755, D02312, 2008.

Nguyen, Q. T., Glasius, M., Sørensen, L. L., Jensen, B., Skov, H., Birmili, W., Wiedensohler, A., Kristensson, A., Nøjgaard, J. K., and Massling, A.: Seasonal variation of atmospheric particle number concentrations, new particle formation and atmospheric oxidation capacity at the high Arctic site Villum Research Station, Station Nord, Atmospheric Chemistry and Physics Discussions, 2016, 1–41, doi:10.5194/acp-2016-205, http://www.atmos-chem-phys-discuss.net/acp-2016-205/, 2016.

Nilsson, E. D., Rannik, U., Swietlicki, E., Leck, C., Aalto, P. P., Zhou, J., and Norman, M.: Turbulent aerosol fluxes over the Arctic Ocean 2. Wind-driven sources from the sea, Journal of Geophysical Research-Atmospheres, 106, 32 139–32 154, 2001.

O'Dowd, C. and de Leeuw, G.: Marine aerosol production: a review of current knowledge, Philosophical Transactions of the Royal Society, 365, 1753–1774, doi:10.1098/rsta.2007.2043, 2007.

O'Dowd, C., Ceburnis, D., Ovadnevaite, J., Bialek, J., Stengel, D., Zacharias, M., Nitschke, U., Connan, S., Rinaldi, M., Fuzzi, S., Decesair, S., Facchini, M., Maullo, S., Santoleri, R., Dell'Anno, A., Corinaldesi, C., Tangherlini, M., and Danovaro, R.: Connecting marine productivity to sea-spray via nanoscale biological processes: Phytoplankton Dance or Death Disco?, Scientific Reports, 5, doi:10.1038/srep14883, 2015.

Orellana, M. V., Matrai, P. A., Leck, C., Rauschenberg, C. D., Lee, A. M., and Coz, E.: Marine microgels as a source of cloud condensation nuclei in the high Arctic, Proceedings of the National Academy of Sciences of the United States of America, 108, 13 612–13 617, 2011.

Ovadnevaite, J., Ceburnis, D., Martucci, G., Bialek, J., Monahan, C., Rinaldi, M., Facchini, M. C., Berresheim, H., Worsnop, D. R., and O'Dowd, C.: Primary marine organic aerosol: A dichotomy of low hygroscopicity and high CCN activity, Geophysical Research Letters, 38, n/a–n/a, doi:10.1029/2011GL048869, http://dx.doi.org/10.1029/2011GL048869, L21806, 2011.

Ovadnevaite, J., Ceburnis, D., Canagaratna, M., Berresheim, H., Bialek, J., Martucci, G., Worsnop, D. R., and O'Dowd, C.: On the effect of wind speed on submicron sea salt mass concentrations and source fluxes, Journal of Geophysical Research: Atmospheres, 117, n/a–n/a, doi:10.1029/2011JD017379, http://dx.doi.org/10.1029/2011JD017379, D16201, 2012.

Ovadnevaite, J., Manders, A., de Leeuw, G., Ceburnis, D., Monahan, C., Partanen, A. I., Korhonen, H., and O'Dowd, C. D.: A sea spray aerosol flux parameterization encapsulating wave state, Atmospheric Chemistry and Physics, 14, 1837–1852, 2014.

Petters, M. D. and Kreidenweis, S. M.: A single parameter representation of hygroscopic growth and cloud condensation nucleus activity, Atmospheric Chemistry and Physics, 7, 1961–1971, doi:10.5194/acp-7-1961-2007, http://www.atmos-chem-phys.net/7/1961/2007/, 2007.

Phinney, L., Leaitch, W. R., Lohmann, U., Boudries, H., Worsnop, D. R., Jayne, J. T., Toom-Sauntry, D., Wadleigh, M., Sharma, S., and Shantz, N.: Characterization of the aerosol over the sub-arctic north east Pacific Ocean, Deep Sea Research Part II: Topical Studies in Oceanography, 53, 2410 – 2433, doi:http://dx.doi.org/10.1016/j.dsr2.2006.05.044, http://www.sciencedirect.com/science/article/pii/S0967064506002025, Canadian SOLAS: Subarctic Ecosystem Response to Iron Enrichment (SERIES), 2006.

Quinn, P. K., Shaw, G., Andrews, E., Dutton, E. G., Ruoho-Airola, T., and Gong, S. L.: Arctic haze: current trends and knowledge gaps, Tellus Series B-Chemical and Physical Meteorology, 59, 99–114, 2007.

Quinn, P. K., Bates, T., Schulz, K., Coffman, D., Frossard, A., Russell, L., Keene, W., and Kieber, D.: Contribution of sea surface carbon pool to organic matter enrichment in sea spray aerosol, Nature Geoscience, 7, 228–232, doi:10.1038/NGEO2092, 2015a.

Quinn, P. K., Collins, D. B., Grassian, V. H., Prather, K. A., and Bates, T. S.: Chemistry and Related Properties of Freshly Emitted Sea Spray Aerosol, Chemical Reviews, 115, 4383–4399, doi:10.1021/cr500713g, pMID: 25844487, 2015b.

Rehbein, P. J. G., Jeong, C.-H., McGuire, M. L., Yao, X., Corbin, J. C., and Evans, G. J.: Cloud and Fog Processing Enhanced Gas-to-Particle Partitioning of Trimethylamine, Environmental Science & Technology, 45, 4346–4352, doi:10.1021/es1042113, pMID: 21488635, 2011.

Rinaldi, M., Decesari, S., Finessi, E., Giulianelli, L., Carbone, C., Fuzzi, S., O'Dowd, C. D., Ceburnis, D., and Facchini, M. C.: Primary and Secondary Organic Marine Aerosol and Oceanic Biological Activity: Recent Results and New Perspectives for Future Studies, Advances in Meteorology, doi:10.1155/2010/310682, 310682, 2010.

Robinson, N. H., Hamilton, J. F., Allan, J. D., Langford, B., Oram, D. E., Chen, Q., Docherty, K., Farmer, D. K., Jimenez, J. L., Ward, M. W., Hewitt, C. N., Barley, M. H., Jenkin, M. E., Rickard, A. R., Martin, S. T., McFiggans, G., and Coe, H.: Evidence for a significant proportion of Secondary Organic Aerosol from isoprene above a maritime tropical forest, Atmospheric Chemistry and Physics, 11, 1039–1050, doi:10.5194/acp-11-1039-2011, http://www.atmos-chem-phys.net/11/1039/2011/, 2011.

Roth, A., Schneider, J., Klimach, T., Mertes, S., vanÂ Pinxteren, D., Herrmann, H., and Borrmann, S.: Aerosol properties, source identification, and cloud processing in orographic clouds measured by single particle mass spectrometry on a central European mountain site during HCCT-2010, Atmospheric Chemistry and Physics, 16, 505–524, doi:10.5194/acp-16-505-2016, http://www.atmos-chem-phys.net/16/505/2016/, 2016.

Schollert, M., Burchard, S., Faubert, P., Michelsen, A., and Rinnan, R.: Biogenic volatile organic compound emissions in four vegetation types in high arctic Greenland, Polar Biology, 37, 237–249, 2014.

Schwarz, J. P., Gao, R. S., Fahey, D. W., Thomson, D. S., Watts, L. A., Wilson, J. C., Reeves, J. M., Darbeheshti, M., Baumgardner, D. G., Kok, G. L., Chung, S. H., Schulz, M., Hendricks, J., Lauer, A., Kärcher, B., Slowik, J. G., Rosenlof, K. H., Thompson, T. L., Langford, A. O., Loewenstein, M., and Aikin, K. C.: Single-particle measurements of midlatitude black carbon and light-scattering aerosols from the boundary layer to the lower stratosphere, Journal of Geophysical Research: Atmospheres, 111, n/a–n/a, doi:10.1029/2006JD007076, http://dx.doi.org/10.1029/2006JD007076, D16207, 2006.

Seuper, D.: ToF-AMS analysis software, http://cires.colorado.edu/jimenez-group/ToFAMSResources/ToFSoftware/index.html, 2010.

Sharma, S., Ishizawa, M., Chan, D., Lavoue, D., Andrews, E., Eleftheriadis, K., and Maksyutov, S.: 16-year simulation of Arctic black carbon: Transport, source contribution, and sensitivity analysis on deposition, Journal of Geophysical Research-Atmospheres, 118, 943–964, 2013.

Shaw, S., Gantt, B., and Meskhidze, N.: Production and Emissions of Marine Isoprene and Monoterpenes: A Review, Advances in Meteorology, 2010, doi:10.1155/2010/408696, 408696, 2010.

Skamarock, W. C., Klemp, J. B., Dudhia, J., Gill, D. O., Barker, D. M., Wang, W., and Powers, J. G.: A Description of the Advanced Research WRF Version 2, Available from NCAR; P.O. BOX 3000; Boulder, CO, 88, 7–25, 2001.

Stohl, A.: Characteristics of atmospheric transport into the Arctic troposphere, Journal of Geophysical Research: Atmospheres, 111, n/a–n/a, doi:10.1029/2005JD006888, http://dx.doi.org/10.1029/2005JD006888, D11306, 2006.

Stohl, A., Forster, C., Frank, A., Seibert, P., and Wotawa, G.: Technical note: The Lagrangian particle dispersion model FLEXPART version 6.2, Atmospheric Chemistry and Physics, 5, 2461–2474, doi:10.5194/acp-5-2461-2005, http://www.atmos-chem-phys.net/5/2461/2005/, 2005.

Tjernström, M., Shupe, M. D., Brooks, I. M., Persson, P. O. G., Prytherch, J., Salisbury, D. J., Sedlar, J., Achtert, P., Brooks, B. J., Johnston, P. E., Sotiropoulou, G., and Wolfe, D.: Warm-air advection, air mass transformation and fog causes rapid ice melt, Geophysical Research Letters, 42, 5594–5602, doi:10.1002/2015GL064373, http://dx.doi.org/10.1002/2015GL064373, 2015GL064373, 2015.

Tunved, P., Ström, J., and Krejci, R.: Arctic aerosol life cycle: linking aerosol size distributions observed between 2000 and 2010 with air mass transport and precipitation at Zeppelin station, Ny-Ã…lesund, Svalbard, Atmospheric Chemistry and Physics, 13, 3643–3660, doi:10.5194/acp-13-3643-2013, http://www.atmos-chem-phys.net/13/3643/2013/, 2013.

Vaattovaara, P., Huttunen, P. E., Yoon, Y. J., Joutsensaari, J., Lehtinen, K. E. J., O'Dowd, C. D., and Laaksonen, A.: The composition of nucleation and Aitken modes particles during coastal nucleation events: evidence for marine secondary organic contribution, Atmospheric Chemistry and Physics, 6, 4601–4616, doi:10.5194/acp-6-4601-2006, http://www.atmos-chem-phys.net/6/4601/2006/, 2006.

Wentworth, G. R., Murphy, J. G., Croft, B., Martin, R. V., Pierce, J. R., Côté, J.-S., Courchesne, I., Tremblay, J.-E., Gagnon, J., Thomas, J. L., Sharma, S., Toom-Sauntry, D., Chivulescu, A., Levasseur, M., and Abbatt, J. P. D.: Ammonia in the summertime Arctic marine boundary layer: sources, sinks and implications, Atmospheric Chemistry and Physics Discussions, 15, 29 973–30 016, doi:10.5194/acpd-15-29973-2015, http://www.atmos-chem-phys-discuss.net/15/29973/2015/, 2015.

Yakobi-Hancock, J. D., Ladino, L. A., Bertram, A. K., Huffman, J. A., Jones, K., Leaitch, W. R., Mason, R. H., Schiller, C. L., Toom-Sauntry, D., Wong, J. P. S., and Abbatt, J. P. D.: CCN activity of size-selected aerosol at a Pacific coastal location, Atmospheric Chemistry and Physics, 14, 12 307–12 317, doi:10.5194/acp-14-12307-2014, http://www.atmos-chem-phys.net/14/12307/2014/, 2014.

Zorn, S. R., Drewnick, F., Schott, M., Hoffmann, T., and Borrmann, S.: Characterization of the South Atlantic marine boundary layer aerosol using an aerodyne aerosol mass spectrometer, Atmospheric Chemistry and Physics, 8, 4711–4728, 2008.

Response to Anonymous Referee # 1

We thank Referee # 1 for their comments and suggestions that have helped to improve this manuscript. Our responses to comments and the corresponding changes to the manuscript are detailed below in blue text.

Major Comments

This paper describes airborne observations of new particle formation in the Canadian Arctic. Increases in small particle number concentrations were observed during low level flights to the east of Resolute Bay on the edge of the main area of sea ice. As the flight continued in open water the particle size distribution evolved and particles increased in size to 50 nm and greater. As these measurements were taken in very clean conditions, in light winds and when the shallow marine boundary layer was capped with a strong inversion the particle evolution can be linked to new particle formation and growth. Chemical measurements of the larger particles show the presence of methyl sulfonic acid (MSA), organic matter and trimethylamine. The organic matter was shown to have a rather different mass spectral chemical signature during the period of particle growth compared to other regions during the study and points to the role of secondary organic matter in growing new particles into particles that may be active as CCN. There may be some evidence that iodine is involved in the new particle formation but the authors, rightly, are tentative in their conclusions on this point. The paper is certainly worthy of publication in ACP in my view if some points are considered.

Page 144-165: Given that a comparison of aerosol number concentration across a range of sizes derived from size distributions and total number concentrations is the central theme to the paper I find it strange that a characteristic size distribution from the UHSAS and SMS and the average integrated number comparison with the CPC is not provided as a figure. This could also be used to illustrate how the integrated number concentrations were derived as well as show the agreement between the different instruments the authors refer to. Size distributions up to 100 nm are shown in figure 3 but I suspect that these are only from the SMS. A characteristic size distribution observed during the case study period has been added as the new Figure 1 in the revised manuscript. Since the UCPC measured particles 5 nm and larger, a comparison of the average integrated concentrations from the UCPC with that of the SMS and UHSAS yields the number of particles between 5 and 20 nm. Therefore, we do not expect the integrated UCPC concentration to agree well with that of the SMS and UHSAS when small particles are present. The agreement mentioned in section 2.3 was in reference to the SMS and UHSAS in their overlapping size range, which is now illustrated in the new Figure 1 and detailed in the text of section 2.3 (see response to specific comments, below).

In the supplementary material (Figure S5), it appears from the profile of Ntotal that there was an initial descent to around 80-100 m and then an ascent to 300 m before the aircraft descended again to 70 m. In this second period of surface layer sampling, Ntotal was not enhanced as it was in the early sampling period. I dont see how this relates to the straight and level runs shown in figure 3 and needs clarifying. We agree that the profile of Ntotal in Figure S5 could be a source of some confusion. Therefore, for consistency with the main text figures, we have replaced the profile of Ntotal with the profile of N_{5-20}. It is correct that there was an initial descent into the lower boundary layer, followed by an ascent to approximately 300 m, before we descended into the lower boundary layer again. This can be seen in the altitude traces shown in Figures 3 and 4 (Figures 4 and 5 in the revised manuscript). As is also evident from the traces of N_{5-20} and N_{20-100} in Figure 3, the total number concentration near 85W is much lower than that near 82W.

Lines 352 to 353 and Figure 3b: "Particle number size distributions illustrate that particles below 20 nm (Figure 3b) grow to form a mode centred at 30 - 40 nm (Figure 3ce)." Size distributions in figures 3b, c and d only show size distributions between 20-100 nm. This needs to be explained clearly in the figure caption and text. I dont think that the authors can say that the size distributions on their own show growth from below 20 nm to form a mode at 30-40 nm. I do not dispute the claim but I would like to see a clearer summary of the evidence presented by the authors in this section to support what is at present simply an assertion. This can be done given the distances and timescales. The advection timescale from 85W to 82W is between 3 and 6 hours at windspeeds 4-8 m/s and the sample time of the aircraft is around 10 minutes depending on the aircraft speed. Given the changes in aerosol concentrations and sizes this excludes a wider aerosol source region and implies that the source is to the west of the sample region and the aerosol distribution develops as the air moves to the east.It would very informative to the reader to include such a discussion at this point in the text in my view and to discount other possibilities. In addition to the above, can the authors say anything about the growth rates of the particles and the size of the condensation sink? We agree that a more clear summary of the evidence for aerosol growth at this point in the text would strengthen this manuscript. To this end, we have expanded the size distributions in Figure 3 (Figure 4 in the revised manuscript) to a range of 20 − 1000 nm by including the UHSAS data. We have also made this clear in the figure caption and text.

We have attempted to estimate the aerosol growth rate from the size distributions observed by the SMS and UHSAS between 82W and 81W (between 86W and 84.4W the number distribution appeared to be dominated by N5-20, with a mode of larger particles of consistent size near 100 nm). Such an estimation is complicated for three main reasons. First, we must estimate the advection time using the average wind speed (6.5 m/s) in the lower boundary layer, neglecting any turbulent motions and potentially underestimating the true transport time. Second, we measured size distributions with SMS (20-100 nm) with a scan time of 60 seconds (40 second up-scan, 20 second down-scan) meaning that we have a total of 10 size distributions over a large spatial area (82W to 81W), and that each size distribution is averaged over a distance of ∼4 km. It is certainly possible for the size distribution to change over 4 km; indeed, we see evidence for this in some size distributions that appear to contain more than one mode below 50 nm. Finally, using these 10 size distributions we must assume that aerosol growth is steady between 82W and

81W, and that the source of condensing material is located at a point to the west of 86W, in order to estimate a growth rate. Under these assumptions, along with the log-normal distribution function method described by Kulmala et al. (2012) and fitting two modes between 20 – 55 nm and 55 – 800 nm, respectively, we find that the mode of smaller particles grew at a rate of 6.6 nm/hr. Additionally, we find the mode of larger particles present between 86–84.4W, peaking at ∼85 nm, decreased in size from 82W to 81W. As noted in section 3.2 the lower boundary layer was characterized by a low pre-existing aerosol surface area of 3.8±2.0 $\mu m^2\,cm^{-3}$, likely assisting particle formation. The apparent decrease in size of this larger mode is likely because smaller particles were growing into larger sizes giving the appearance of a decrease in the geometric mean diameter above 55 nm. We believe that this relatively large estimated growth rate carries a significant uncertainty for the reasons described above, and therefore have chosen not to include this estimation in the manuscript.

To reflect these points, we have modified the first paragraph (second paragraph in the revised manuscript) of section 3.2 as follows: " Particle number size distributions from 20 – 1000 nm illustrate that particles below 20 nm (Figure 4a,c) grow to form a mode centred at 30 – 40 nm (Figure 4d–f). Beyond 86W we observe N_{20-100} at background levels of ∼100 cm^{-3}. These observations suggest that the aerosol size distribution develops as the airmass moves downwind to the east. The advection time scale from 85.8 – 81.1W is 6.7 hr, given an average wind speed of 6.5 m/s, and the sampling time of the aircraft over this distance is 35 min. Given the substantial changes in aerosol size and number concentration observed over this relatively short time period, our observations suggest that a source of condensible material contributing to aerosol growth is present to the west of the sampling region and a wider source region is unlikely to contribute to these observed changes. Any estimate of the growth rate in this case is associated with a large uncertainty, since it is complicated by a number of factors including the one-minute time resolution of the SMS that corresponds to a sampling distance of ∼4 km, and uncertainties in the advection time. Therefore, it is difficult to quantitatively follow the evolution of the size distribution. Compounded by our lack of knowledge of the spatial uniformity of the condensible material, we do not present an estimate of the growth rate here."

Lines 368-372: Elevated concentrations of larger particles and aerosol component mass are observed at the east of the sample region at altitudes up to 900 m. The authors suggest that some mixing has occurred. The thermodynamic profiles of potential temperature in figure S5 show an increase with height from the surface to around 300 m, no change to 500 m, and a further increase aloft. This suggest the lowest layer remains stable to 300 m and there is little thermodynamic forcing of mixing throughout the column. Was any cloud present through the column, the RH profile suggest not, but without cloud it is rather difficult to see how mixing of the surface layer could be responsible for the profiles observed. This flight took place largely under clear sky conditions, and there was no cloud that could have contributed to mixing in this case. FLEXPART-WRF suggests some downslope flow off Devon Island that could have created some mixing in hours prior to our measurements, and wind directions shift slightly as we move above the lower boundary layer, from west towards north-west. This is consistent with the results from

WRF. We do agree that the thermodyanmic profiles do not suggest mixing has occurred, and we have altered this discussion as follows: "$N_{>50}$, $N_{>100}$ and CCN concentrations remain somewhat elevated up to ∼900 m (Figure 4b, near 80.5W), suggesting that some mixing above the lower boundary layer occurred during some time prior to our observations, possibly due to katabatic winds off Devon Island suggested from the Flexpart analyses (Figure 3c). Profiles of aerosol number and composition are presented in Figure S5 in the Supplement."

Minor Comments

Line 121: isn't the inner diameter the most important? Thank-you for catching this error, this information has been added to the sentence as follows: "Aerosol flowed into the cabin through a stainless steel manifold (outer diameter = 2.5 cm, inner diameter = 2.3 cm) and was directed to the various particle instruments..."

Lines 155-157: The authors state that the agreement between different aerosol instruments was generally within a factor of two. What was within a factor of two, total number, size or something else? The comment needs to be more precise. This sentence has been revised to: "Particle number concentrations from the SMS and UHSAS generally agreed within a factor of two over their overlapping size range (70 – 100 nm)."

Line 156: The CCNC is not mentioned at all in the text up to this point. I assume that this is a cloud condensation nucleus counter but the model and operating mode is not mentioned, was it run at one or more supersaturations or was it scanned, if so over what timescale and over what supersaturation range? The Cloud Condensation Nuclei Counter (CCNC) is described in section 2.4. This reference to the CCNC in section 2.3 has been removed for clarity. The CCNC was operated at 0.6% supersaturation, as described in section 2.4.

Line 269-270: why two laser beams? are these separated or is the sample volume of the two co-located? The two laser beams are separated so that the particle time-of-flight can be measured, and the particle vaccum aerodynamic diameter can be determined. This sentence has been revised to: "The particles are detected and sized by light scattering when passing two continuous laser beams separated along the path of the sampled aerosol."

Page 28: Figure 2 caption: "The location of the aircraft during sampling is noted by the grey triangle" I assume the grey triangle refers to the position of the aircraft at the time of the start of the FLEXPART release? Yes, this is also the location of the FLEXPART release shown in Figure 2. This portion of the figure caption has been revised for clarity as follows: "The aircraft location at the time of the FLEXPART-WRF particle release is indicated with a grey triangle ..."

Line 305 and following: It would be useful to provide some detail on the time of take-off and the air speed and/or time of the profiles and manoeuvres. We have added information on the time at which the aircraft covered the study area, in the first paragraph of section 3.1, as follows: "The relevant portion of this flight, over open water in Lancaster Sound, is highlighted in Figure 2a (79.7W to 86.5W, 20:00 – 21:20 UTC). During this time the aircraft flew to the west below 100 m a.g.l. and covered a distance of approximately 175 km at a survey speed of 75 m/s under clear sky conditions."

Table S1: The ion m/z are incorrect for CH3SO+ and CH3SO2+ This error has been corrected.

Figure S5: caption, should read "below the inversion" and not "in the inversion" This has been changed.

Line 350: "of" not "on" This error has been corrected.

Page 11-12: Figure 6: Given the very low particle numbers the ALABAMA instrument is limited by counting statistics. It is rather disingenuous to provide the cluster abundances as a fraction when the total numbers in each cluster are less than the fractional amount. It is better to show the total numbers of particles counted. By my calculation, only the TMA containing cluster includes more than 10 particles in the cluster and many of the "clusters" are only 1, 2 or 3 particles. The legend in part (a) of this figure has been changed to show the total particle number, and the total number of spectra is now indicated in the legend. For clarity, the reference to "clusters" or "classes" has also been removed from this figure caption since particles were manually grouped based on the presence of marker peaks, as described in section 2.6.3.

Figure S6: It is probably best to present the 4 point smoothing and the uncertainty based on the Poisson counting stats which I suspect will show there is little that is statistically significant above 200 nm. We have replaced the 4-point smoothing with the log-normal fits to the size resolved data for total organic aerosol and sulfate during the case study period. These log normal fits show a clear modes at 122 nm and 140 nm for organics and sulfate, respectively. These log-normal fits also show that there is little that is statistically significant above 200 nm.

Lines 451-453: I am unconvinced that the ammonium shows a smooth decrease from west to east similar to the sulfate. There is a marked reduction in ammonium in the western boundary layer that is not matched by the sulfate. Our intention here was to highlight the observation that ammonium shows some correlation with both organic and inorganic species. To make this point clearer, this sentence has been revised as follows: "Ammonium concentrations are low and show some correlation with organic and inorganic aerosol species, suggesting that OA, MSA and sulfate could be partially neutralized by ammonium."

References

Kulmala, M., Petäjä, T., Nieminen, T., Sipilä, M., Manninen, H. E., Lehtipalo, K., Dal Maso, M., Aalto, P. P., Junninen, H., Paasonen, P., Riipinen, I., Lehtinen, K. E. J., Laaksonen, A., and Kerminen, V.-M.: Measurement of the nucleation of atmospheric aerosol particles, Nat. Protocols, 7, 1651–1667, URL `http://dx.doi.org/10.1038/nprot.2012.091`, 2012.

Response to Anonymous Referee # 2

We thank Referee # 2 for their helpful comments on this manuscript. Our responses to comments and the corresponding changes to the manuscript are detailed below in blue text.

General Comments

The manuscript "Growth of nucleation mode particles in the summertime Arctic: a case study" by Willis et al., describes physicochemical properties of atmospheric nanometersized particles during a summertime new particle formation event in the Canadian Arctic Archipelago. As the authors correctly point out, new particle formation events, which can form in summer in the Arctic due to clean conditions and higher photochemical activity, are considered to be an important source of cloud condensation nuclei in this region. Because of this, knowledge of the sources and mechanisms of these events are important in order to assess the coupling between terrestrial processes and the atmospheric hydrological cycle. This study makes an important contribution this understanding by providing high quality measurements. They are presently clearly, and in a well-organized manner. I cannot find many flaws in this study and manuscript; however since it is my job to provide helpful comments I offer the following suggestions that I hope might improve the overall quality of this manuscript.

1. Since the air mass for this day has spent a week over land (Devon Island), it would be helpful for the reader to know the nature of the land surface and possible sources of condensible gas precursors. According to MODIS land cover data (Friedl et al., 2010), as well as visual observations made during the campaign, Devon Island is covered by snow and ice. As mentioned in section 3.3.1, a photochemical source of volatile organic compounds from snow and ice is a potential source that cannot be discounted. However, our observations of methanesulfonic acid and trimethylamine suggests a significant marine contribution. We have added information on the nature of the land cover on Devon Island to section 3.1 and the relevant figure caption, to illustrate other possible sources of condensible gas precursors.

2. Figures 3 and 4. In the text, the authors discuss the lack independent behavior of the number concentrations of particles larger than 50 nm and those between 5 and 20 nm. That difference is best depicted by including the latter on top of the stack of plots in Figure 4. Not such a big deal, but it would allow for closer comparison of the differences between these distributions. We agree that rearranging the figures in this way would improve the clarity of our discussion. All particle number traces (previously separated between Figures 3 and 4) are now included in one figure, and consequently all composition information from the HR-ToF-AMS is now included in one figure (previously separated between Figure 4 and 5).

3. Figures 3 b-e show steady growth of the nucleation mode as the aircraft samples downwind. Since "growth" is such a critical aspect of this manuscript (the word appears 52 times in this manuscript), this reader at least is interested

in seeing an estimate of the growth rate. This should be feasible given the steady wind conditions and data obtained in this study. We certainly agree that growth in an important aspect of this manuscript. We have attempted to estimate the aerosol growth rate from the size distributions observed by the SMS and UHSAS between 82W and 81W (between 86W and 84.4W the number distribution appeared to be dominated by N5-20, with a mode of larger particles of consistent size near 100 nm). Such an estimation is complicated for three main reasons. First, we must estimate the advection time using the average wind speed (6.5 m/s) in the lower boundary layer, neglecting any turbulent motions and potentially underestimating the true transport time. Second, we measured size distributions with SMS (20-100 nm) with a scan time of 60 seconds (40 second up-scan, 20 second down-scan) meaning that we have a total of 10 size distributions over a large spatial area (82W to 81W), and that each size distribution is averaged over a distance of ∼4 km. It is certainly possible for the size distribution to change over 4 km; indeed, we see evidence for this in some size distributions that appear to contain more than one mode below 50 nm. Finally, using these 10 size distributions we must assume that aerosol growth is steady between 82W and 81W, and that the source of condensing material is located at a point to the west of 86W, in order to estimate a growth rate. Under these assumptions, along with the log-normal distribution function method described by Kulmala et al. (2012) and fitting two modes between 20 − 55 nm and 55 − 800 nm, respectively, we find that the mode of smaller particles grew at a rate of 6.6 nm/hr. Additionally, we find the mode of larger particles present between 86–84.4W, peaking at ∼85 nm, decreased in size from 82W to 81W. This is likely because smaller particles were growing into larger sizes giving the appearance of a decrease in the geometric mean diameter above 55 nm. We believe that this relatively large estimated growth rate carries a significant uncertainty for the reasons described above, and therefore have chosen not to include this estimation in the manuscript.

4. Figure 6: correct x-axis to show more clearly the range of particle diameter (it appears that the range starts with sub-10 nm diameters). Also, if the diameter is on the x-axis starts at 300 nm, and the minimum detectable size is 150 nm, then why weren't smaller particles detected by ALABAMA? The x-axis of Figure 6 has been corrected to more clearly show its range. Due to limitations of the ALABAMA's optical detection and the transmission efficiency of the aerodynamic lens, the ALABAMA detection efficiency depends on size. Particles at approximately 400 nm are detected most efficiently, and particles smaller than approximately 300 nm have a much lower detection efficiency. Some particles down to 150 nm were detected during this flight. But, during the case study period very few particles between 150 and 300 nm were detected by the ALABAMA. The description of the ALABAMA size range (Section 2.6.3) has been modified for better clarity as follows: "Optical detection of aerosol limits the minimum detectable particle size to approximately 150 nm with particles at approximately 400 nm detected at the highest efficiency. The transmission efficiency in the aerodynamic lens limits the maximum detectable size to approximately 1000 nm."

Specific Comments

Minor editorial comment: For consistency, change the spelling of "sulfate" in Figure 4. This error has been corrected.

References

Friedl, M., Sulla-Menashe, D., Tan, B., Schneider, A., Ramankutty, N., Sibley, A., and Huang, X.: MODIS Collection 5 global land cover: Algorithm refinements and characterization of new datasets, Collection 5.1 IGBP Land Cover, 2010.

Kulmala, M., Petäjä, T., Nieminen, T., Sipilä, M., Manninen, H. E., Lehtipalo, K., Dal Maso, M., Aalto, P. P., Junninen, H., Paasonen, P., Riipinen, I., Lehtinen, K. E. J., Laaksonen, A., and Kerminen, V.-M.: Measurement of the nucleation of atmospheric aerosol particles, Nat. Protocols, 7, 1651–1667, URL http://dx.doi.org/10.1038/nprot.2012.091, 2012.

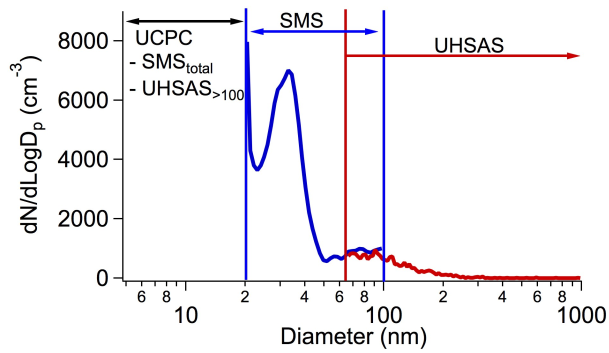

Figure 1. Characteristic size distribution showing the size range of the SMS and UHSAS (observed near 81.1° W in Lancaster sound, see Figure 2a) . Number concentrations from 5 to 20 nm (N_{5-20}) were estimated by subtracting the sum of the SMS total number concentration (N_{20-100}) and UHSAS number concentration greater than 100 nm ($N_{>100}$) from the total UCPC concentration (i.e., $N_{>5}$).

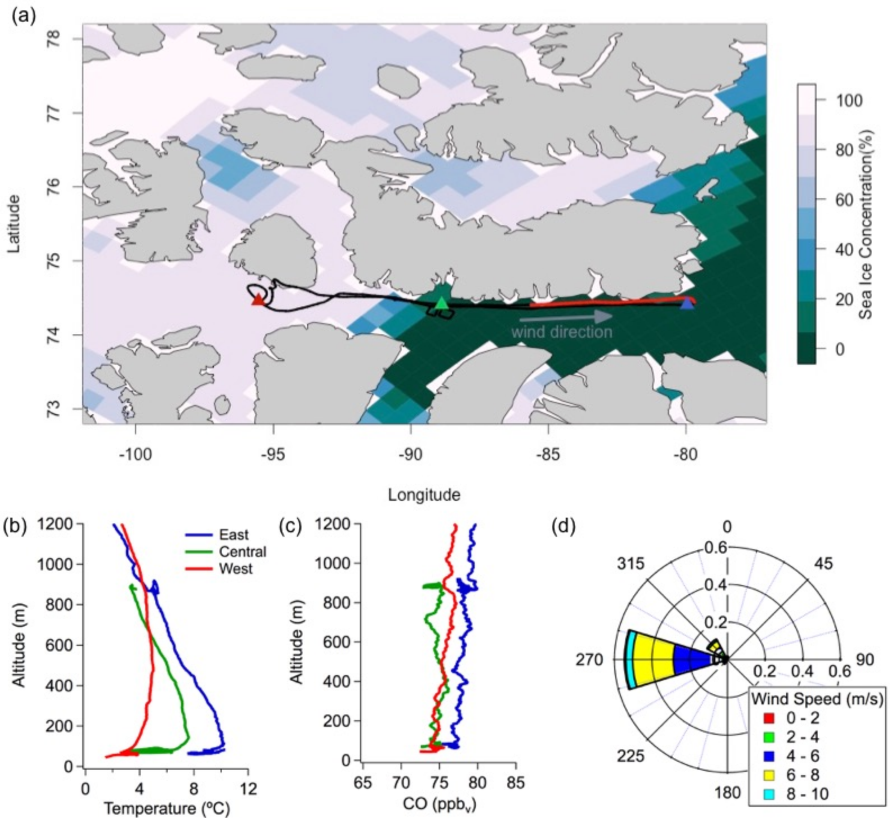

Figure 2. (a) Map of the study area showing sea ice concentration for 12 July 2014 from the National Snow and Ice Data Center (nsidc.org, (Cavalieri et al., 1996)) and the flight track originating at Resolute Bay, Nunavut (74° 41' N, 94° 52' W) and extending to eastern Lancaster Sound. The case study area is highlighted in red (20:00 – 21:20 UTC, 79.7° W to 86.5° W), at which time the aircraft travelled westward below ∼100 m a.g.l. The prevailing wind direction is marked with an arrow. Triangles mark the location at which the aircraft reached ∼1 km a.g.l during each profile shown in (b) and (c). (b) and (c) Profiles of temperature and CO mixing ratio near Resolute Bay (red), in central Lancaster Sound (green) and in eastern Lancaster Sound (blue). (d) Flight-average wind rose, wind speeds at the surface averaged ∼ 6.5 $\mathrm{m\,s^{-1}}$.

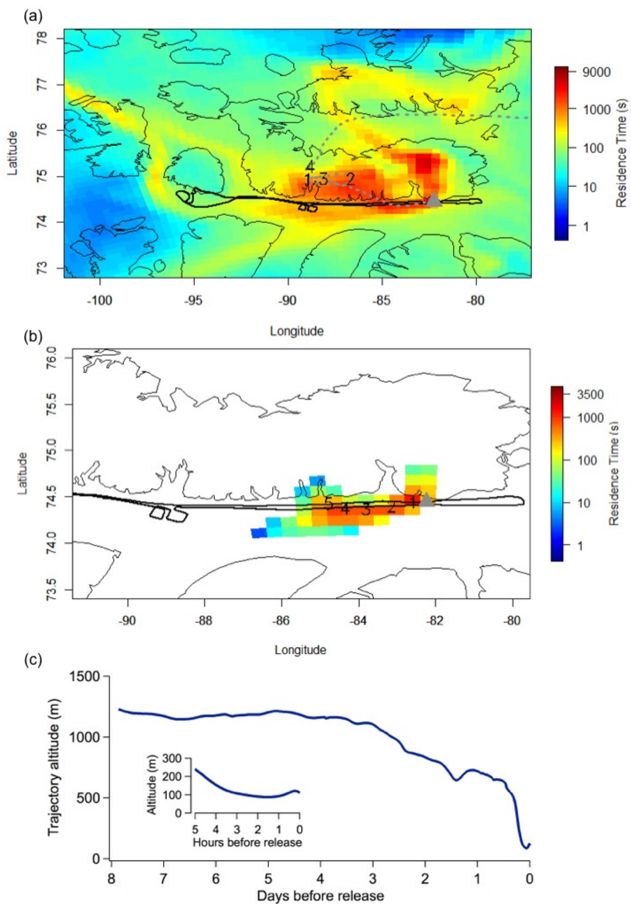

Figure 3. (a) Total column airmass residence time predicted by FLEXPART-WRF, indicating the origin of air sampled along the flight track. The aircraft location at the time of the ~~aircraft during sampling is noted by the grey triangle, which also indicates the~~ FLEXPART-WRF particle release ~~location~~ is indicated with a grey triangle (74.4° N, 82.2° W, ∼85 m a.g.l., 20:39:25 UTC). The color scale represents the residence time of air, in seconds, at a particular location before arriving at the aircraft position. The plume centroid location is shown with a grey dashed line. Numbers indicate the plume centroid location, in days prior to release. (b) Partial column (below 300 m) PES predicted by FLEXPART-WRF shown as residence time in seconds for particles released at the aircraft location in (a). The color scale shows the residence time particles for five hours prior to the release time and below 300 m. Numbers indicate the plume centroid location, in hours prior to release. (c) Plume centroid altitude eight days prior to release and five hours prior to release (inset).

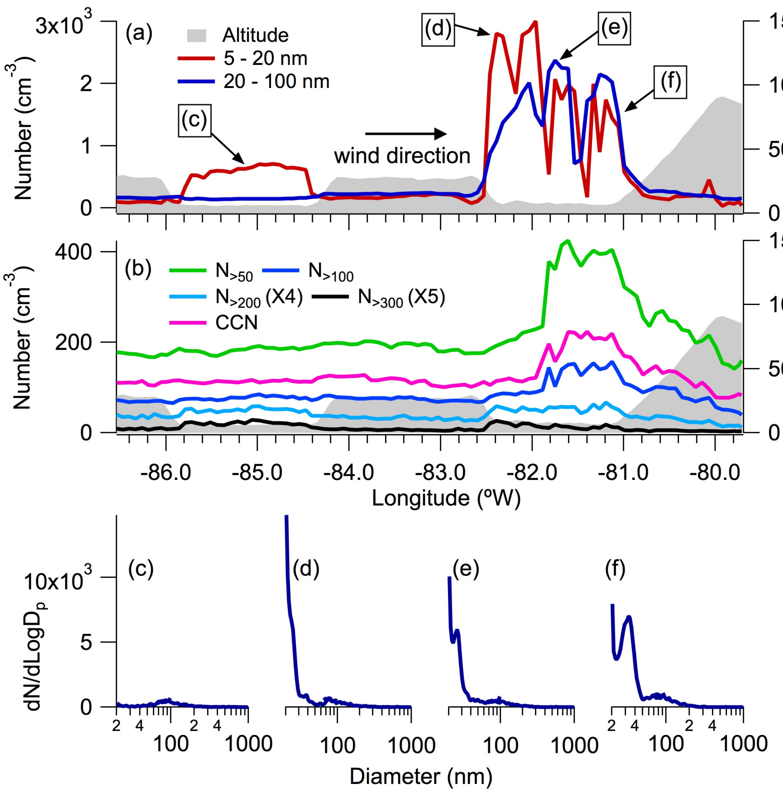

Figure 4. (a) Aircraft altitude (grey) and particle number concentrations from 5 – 20 nm (N_{5-20}, red) and 20 – 100 nm (integrated SMS concentration, N_{20-100}, dark blue), both shown at the time resolution of the SMS, over the case study area highlighted in Figure 2a. (b) Particle number concentrations greater than 50 nm ($N_{>50}$, light green), greater than 100 nm ($N_{>100}$, dark blue), greater than 200 nm ($N_{>200}$, light blue, multiplied by four), greater than 300 nm ($N_{>300}$, black, multiplied by five) and CCN concentrations at 0.6% supersaturation (pink) shown at the time resolution of the SMS. Particle-number size distributions from ~~20 to 100 nm~~ 20 to 1000 nm (from the SMS and UHSAS) at (c) 85.1 ° W, (d) 82.3° W, (e) 81.8° W and (f) 81.1° W.

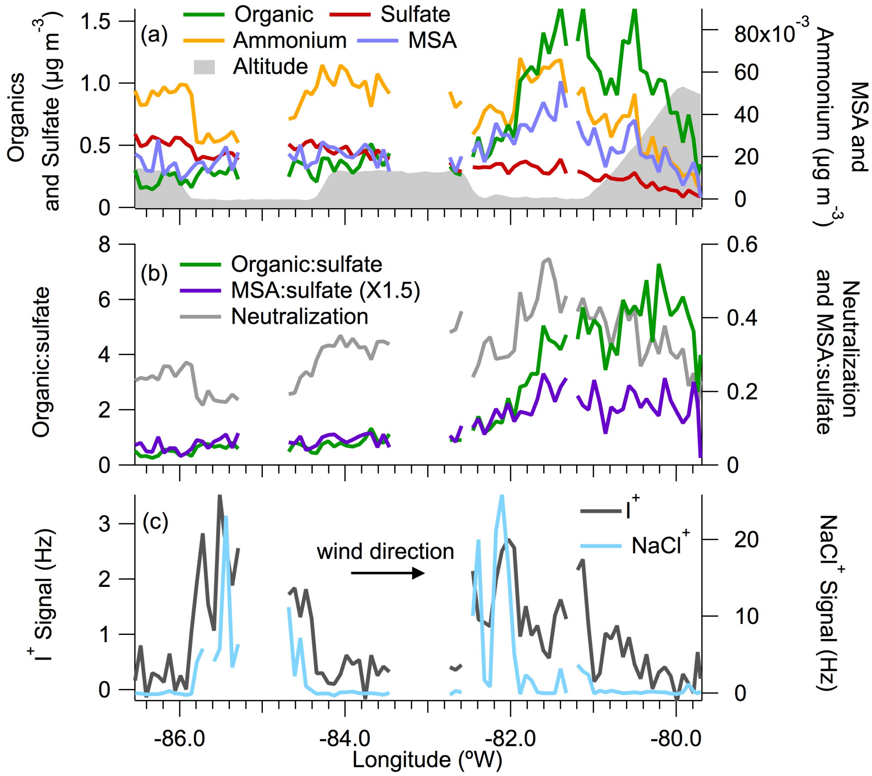

Figure 5. (a) Organic species, sulfate, ammonium and methanesulfonic acid (MSA) measured by the HR-ToF-AMS, over the case study area highlighted in Figure 2a. Altitude is shown in grey on the same scale as Figure 4. (b) Organic-to-sulfate ratio (green), MSA-to-sulfate ratio (purple) and extent of neutralization (grey). The extent of neutralization is the ratio of measured to predicted ammonium, based on measured sulfate, nitrate and MSA. (c) I^+ (m/z 126.90) and $NaCl^+$ signal from the HR-ToF-AMS.

~~Organic-to-sulfate ratio (green), MSA-to-sulfate ratio (purple) and extent of neutralization (orange) over the case study area highlighted in Figure 2a. Altitude is shown in grey on the same scale as Figure 4 and **??**. The extent of neutralization is the ratio of measured to predicted ammonium, based on measured sulfate, nitrate and MSA.~~

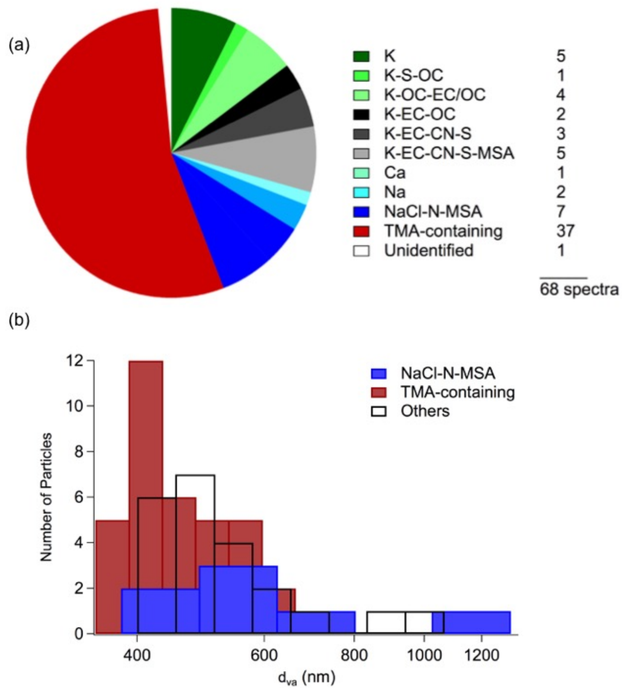

Figure 6. (a) Pie chart depicting particle ~~classes~~ types detected by the ALABAMA over the case study area highlighted in Figure 2a~~, with~~. Particles were grouped based on the presence of marker peaks and the particle ~~class names indicating~~ group name indicates the relative abundance of the corresponding signals in particle spectra. A total of 68 particle spectra were obtained during the approximately two-hour period~~; 37 particles contained detectable trimethylamine (TMA) signal and 7 particles contained markers for sea salt ()~~. TMA-containing particles are mostly internally mixed with K, S, OC and to a lesser degree with MSA and EC/OC. Not all TMA-containing particles included signal for MSA; 13% of all detected particles contained both TMA and MSA signals. (b) Size distributions (in terms of vacuum aerodynamic diameter, d_{va}) of TMA-containing particles (red), NaCl-containing particles (blue), and all other particles classes (transparent).

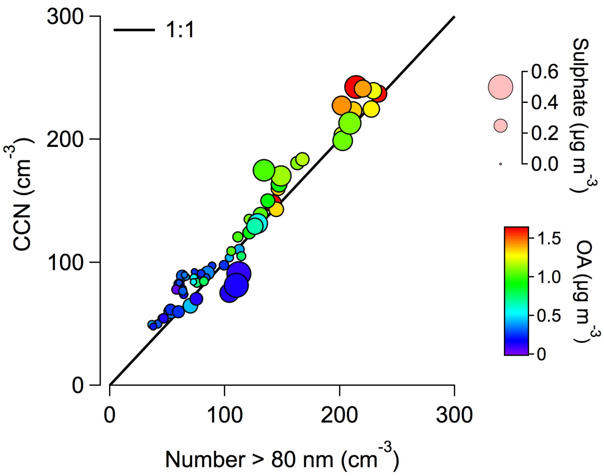

Figure 7. Correlation between the number of particles greater than 80 nm ($N_{>80}$, measured by the UHSAS) and the cloud condensation nuclei concentration (CCN) at 0.6% supersaturation, below 1 km, during the case study period. Data are coloured by organic aerosol loading and point size corresponds to sulfate loading.